The effect of water on Si and O diffusion rates in olivine and implications for transport properties and processes in the upper mantle

Fidel Costa, Sumit Chakraborty

HAL Id: hal-00532129
https://hal.science/hal-00532129

Accepted Manuscript

Title: The effect of water on Si and O diffusion rates in olivine and implications for transport properties and processes in the upper mantle

Authors: Fidel Costa, Sumit Chakraborty

Please cite this article as: Costa, F., Chakraborty, S., The effect of water on Si and O diffusion rates in olivine and implications for transport properties and processes in the upper mantle, *Physics of the Earth and Planetary Interiors* (2007), doi:10.1016/j.pepi.2007.10.006

The effect of water on Si and O diffusion rates in olivine and implications for transport

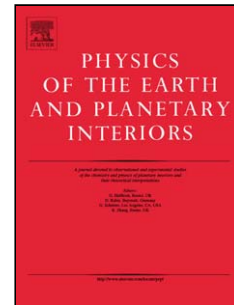**properties and processes in the upper mantle**

Fidel Costa*

Institut für Geologie, Mineralogie & Geophysik, Ruhr-Universität, Bochum. Bochum 44780,

Germany

and

CSIC, Institut de Ciències de la Terra 'Jaume Almera', Lluís Solé i Sabarís s/n, 08028
Barcelona, Spain

Sumit Chakraborty

Institut für Geologie, Mineralogie & Geophysik, Ruhr-Universität, Bochum. Bochum 44780,

Germany

*corresponding author
CSIC
Institut de Ciències de la Terra 'Jaume
Almera'
Lluís Solé i Sabarís s/n
08028 Barcelona
Spain
Tel: ++34 93 4095410 (ext. 265)
Fax: ++34 93 4110012
email: fcosta@ija.csic.es

Sumit Chakraborty
Institut für Geologie, Mineralogie, und
Geophysik
Ruhr-Universität, Bochum
Bochum 44780
Germany
Tel ++49 234 322 4395
Fax ++49 234 321 4433
e-mail: Sumit.Chakraborty@rub.de

1 **Abstract**

2 We performed piston cylinder experiments (1200 - 1350 ^{o}C, 2 GPa) to determine the diffusion

3 rates of Si and O in mantle olivine under water undersaturated (brucite absent, 45 ppm H_2O in

4 olivine) as well as close to water-saturated (brucite present, ~370 ppm H_2O in olivine)

5 conditions. Diffusion couples consisted of oriented and polished San Carlos olivine cylinders

6 coated with thin (~ few 100 nm) films of the same composition enriched in ^{29}Si and ^{18}O, with

7 a protective coating of ZrO_2 on top. Relationships between water solubility in olivine and

8 water fugacity, combined with thermodynamic equilibrium calculations, indicate $fH_2O \sim 1$

9 GPa, $fO_2 \sim$ IW buffer for brucite absent and $fH_2O \sim 9$ GPa, $fO_2 \sim$ QFM buffer for brucite

10 present experiments. We find that under hydrous conditions $D_{Si} \approx D_O$ and diffusion anisotropy

11 is weak to non-existent. Fitting the raw data at 2 GPa and $fH_2O \sim 0.93$ GPa yields Arrhenius

12 parameters [D_o and E_p in $D = D_o \exp(-E_p/RT)$] of: 1.68 ($\pm$3.52) • 10^{-7} m^{2}s^{-1} and 358 $\pm$ 28

13 kJmol^{-1} for Si, and 1.43 ($\pm$1.80) • 10^{-4} m^{2}s^{-1} and 437 $\pm$ 17 kJmol^{-1} for O, respectively (1 sigma

14 errors). D (2 GPa, $fH_2O = 0.97$ GPa, 1200 ^{o}C) : D (1 atmosphere, dry, 1200 °C) is 1000 for Si

15 and 10 for O, respectively. Equations incorporating explicitly the effect of water are discussed

16 in the text.

17 Analysis of our data suggests that O diffuses by an interstitial mechanism whereas Si

18 diffuses via vacancy complexes. The relation between the water fugacity and the Si diffusion

19 rates seems to obey a power law with a water fugacity exponent of 0.2 to 1. The amount of H

20 incorporated into olivine at the experimental conditions is orders of magnitude higher than the

21 likely concentration of Si vacancies. Therefore, a small fraction (~ 0.01%) of the total

22 incorporated H in olivine suffices to considerably enhance the concentration of Si vacancies,

23 and hence diffusion rates. Activation energies for O diffusion under dry and wet conditions

24 are similar, indicating that the mechanism of this diffusion does not change in the presence of

25 water. This inference is consistent with results of computer simulations.

26   Dislocation creep in olivine under wet conditions appears to be controlled by both, Si as

27   well as O diffusion. Absolute creep rates can be calculated from the diffusion data if it is

28   assumed that climb and glide of dislocations contribute equally to creep. Finally, analysis of

29   the various transport properties indicate that < 10 ppm of water in olivine is sufficient to cause

30   a transition from "dry" to "wet" laws for most processes. As these water contents are even

31   lower than the observed water contents in most mantle olivines (i.e. minimum values

32   measured at the surface), we conclude that results of water present but undersaturated kinetic

33   experiments are directly applicable to the mantle. Indeed, "wet" kinetic laws should be used

34   for modeling geodynamic processes in the upper mantle, even if the mantle is thought to be

35   undersaturated with respect to water.

36

37   **Key words:** diffusion, water, deformation, olivine, silicon, oxygen, creep, mantle,

38   experiment, nominally anhydrous mineral (NAM), transport.

39

40

41   **1. Introduction**

42   Water plays a crucial role in most biological, atmospheric, and surface geological

43   processes. But it also has a large effect on the physical properties of materials and processes

44   that occur deeper within the Earth. Experimental results in the last two decades show that

45   even small amounts (< 0.005 wt%) of H in nominally anhydrous minerals (NAMs) such as

46   olivine or pyroxenes decreases the melting temperature and viscosity of the mantle, and

47   enhances electrical conductivity and chemical diffusivity in it (e.g., Mei and Kohlstedt, 2000;

48   Bolfan-Casanova, 2005; Hier-Majumder et al., 2005; Hirschmann, 2006; Karato, 2006;

49   Yoshino et al. 2006; Wang et al., 2006; Demouchy et al., 2007). Despite the information that

50   already exists, one can identify three main areas where more work is required:

51   (1) A robust quantification of the relation between the H content and the different physical

52   properties at the relevant conditions does not exist. Measuring the rheological behavior of

53   mantle material in the presence of water at upper mantle pressures remains a daunting

54   challenge, with only two data sets obtained above 300 MPa (e.g., Hirth and Kohlstedt, 2003;

55   Karato and Jung, 2003). However, precise relations between the "wet" vs. "dry" flow of these

56   materials at high pressures are necessary to understand the factors that determine the nature of

57   plate tectonics (e.g., Lithgow-Bertelloni and Richards, 1995; Hirth and Kohlstedt, 1996;

58   Billen and Gurnis, 2001; Bercovici and Karato, 2003; Regenauer-Lieb, 2006).

59   (2) The mechanistic connection between H incorporation and changes in the different

60   transport properties such as ionic diffusion, deformation, and electrical conductivity remains

61   unclear. Diffusion data in water-bearing olivine is limited to Fe-Mg (Hier-Majumder et al.

62   2005) and it is not directly related to deformation or electrical conductivity. Computer

63   simulations (e.g., Brodholt and Refson, 2000; Walker et al., 2003; Wright, 2006), water

64   solubility measurements (e.g., Bai and Kolstedt, 1992; Kohlstedt et al., 1996; Keppler and

65   Bolfan-Casanova, 2006), and spectroscopic studies of NAMs (e.g., Beran and Putnis, 1983;

66   Beran and Libowitzky, 2006; Kohn, 2006) have contributed much to indicate the possible

67   location of H in the olivine structure, but the results are far from conclusive.

68   (3) It is necessary to quantify at what H concentration the physical and chemical behavior

69   of mantle materials change from the dry to the water-bearing mechanisms / rates, and if such

70   concentrations are likely to be present in the upper mantle. Studies of mantle xenoliths

71   indicate that NAMs contain significant but very variable amounts of H (a few to a few

72   hundred ppm; e.g., Bell and Rossman, 1992; Ingrin and Skogby, 2000). These water contents

73   are typically lower than those at which the experimental data on physical properties are

74   acquired. Nonetheless, evidence from modeling the mantle flow under the western U.S. seems

75   to require a 'wet' rheological law (Dixon et al., 2004; Freed and Bürgmann, 2004).

4

76   Here we present experimental data on Si and O diffusion rates in mantle olivine in the

77   presence of H, and use these results to address some of the points above. We first explain in

78   some detail the experimental and analytical strategy we have used. Next, the diffusion data

79   are presented and the influence of the different intensive variables on the kinetic parameters

80   are disentangled. The results are then discussed within the context of existing point defect

81   thermodynamic models of olivine and related to Fe-Mg diffusion and dislocation creep rates

82   of mantle olivine.

83

84   **2. Experimental and analytical approach**

85   One the of the main challenges of the experiments was to ensure mechanical as well as

86   chemical stability of olivine and of the diffusion couple (crystal plus thin film) during the

87   water-bearing, high pressure and temperature annealing conditions. Thus, we describe below

88   in some detail the problems encountered before reaching the final working configuration.

89

90   *2.1 Starting materials and diffusion couples*

91   San Carlos olivine crystals free of cracks or inclusions were selected and oriented parallel to

92   one of the crystallographic axes using optical methods on a spindle stage. The orientations of

93   some of these crystals were determined *a posteriori* using the EBSD technique (electron

94   backscatter diffraction) on a scanning electron microscope and differences between the two

95   methods were < 10 degrees. The oriented crystals were cut into 1 to 2 mm thick slices and

96   polished using diamond compounds followed by the combined mechano-chemical action of a

97   highly alkaline colloidal silica solution (OP-S of Struers). We used cylinders that were drilled

98   out of the olivine slices with a diameter of ~ 2.5 mm and thickness of 1 to 2 mm.

99   The polished surfaces of the olivine cylinders were deposited with thin films (200 - 1000

100   nm thick) of the same olivine major element composition but doped with ^{18}O and ^{29}Si using

101   the pulsed laser deposition facility available at the Institute of Geology, Mineralogy and

102   Geophysics at Ruhr-Universitat Bochum (Dohmen et al., 2002a, and 2007). It was found that

103   recrystallization, grain growth or dissolution during annealing destroyed the olivine thin film.

104   This was overcome by depositing a second protective layer that would act inertly; after

105   several tests a film of ZrO_2 was found to be ideal for this purpose (Fig. 1a). Moreover, to

106   minimize surficial effects and reaction with the environment, two such doubly coated crystals

107   were placed on top of each other in a "sandwich" geometry (Fig. 1b). With this approach we

108   also obtained two olivine crystals from each experiment in which diffusion profiles could be

109   measured, and this provided a check of the internal consistency and reproducibility of data.

110   **FIGURE 1**

111   *2.2 Experimental techniques*

112   All experiments were performed in an end-loaded piston cylinder. The observed pressure

113   was found to be within 0.2 GPa of the quartz-coesite transition reported by Bose and Ganguly

114   (1995a). Temperatures were monitored using a W_{25}-Re_{75} thermocouple and no pressure

115   correction was made to the thermocouple readings. All experiments were performed at 2 GPa

116   and over a temperature range of 1200 to 1350 $^{\circ}$C at 25 $^{\circ}$C intervals (Table 1).

117   The cell assembly (Fig. 2) is similar to other high pressure diffusion experiments in the

118   piston cylinder (Elphick et al., 1985; Chakraborty and Ganguly, 1992). The main problems

119   that we encountered were to find an assembly that was soft and unreactive with the olivine

120   and thin film under water-present conditions. We tested several capsule materials including,

121   NaCl, Ni, Mo, and $Au_{75}Pd_{25}$, since these were successful in previous experiments (e.g.,

122   Goldsmith, 1991; Graham and Elphick, 1991; Chakraborty and Rubie, 1996; Kohlstedt et al.,

123   1996; Pichavant *et al*., 2002). It was found that NaCl corroded the olivine surface, whereas

124   the Ni, Mo and AuPd were not soft enough and the crystals were recovered completely

125   crushed. To try to overcome this we surrounded the crystals with brucite and talc as in the set

126   up used in the water solubility in olivine experiments of Kohlstedt et al. (1996). However,

127   contrary to the observations of Kohlstedt et al. (1996) at lower temperatures (~ 1100 °C),

128   many of our crystals completely reacted with the surroundings due to the higher temperatures

129   that we need to induce significant diffusion (1200 to 1350 $^{\circ}$C). In the experiments where

130    $Au_{75}Pd_{25}$ capsules were in direct contact with the olivine it was found using Rutherford

131   Backscatter Spectroscopy (RBS) that the crystal had changed its composition within the first

132   few tens of nm of its surface (the region of our interest) due to Fe loss to the capsule. Thus,

133   although for many purposes Fe loss with this type of material is negligible (e.g., Pichavant *et*

134   *al*., 2002) it is not the case when studying concentration differences at the nanometer scale.

135   Finally, two capsule setups were successful. The crystals were set in a graphite matrix and

136   graphite capsule, or they were set in a graphite inner capsule surrounded by a brucite powder

137   and this was enclosed in a welded $Au_{75}Pd_{25}$ outer capsule. Using these setups we were able to

138   recover undamaged single crystals of olivine, but the pressure and temperature range that can

139   be investigated is limited by the stability of orthopyroxene + magnesite relative to olivine +

140   graphite. SEM images of some early runs (Fig. 2) clearly demonstrate the consequences of

141   crossing this reaction boundary. In most experiments we did not explicitly add water, but

142   these nominally "dry" runs were found to be water-bearing, and the source of water was the

143   talc of the cell assembly (Fig. 3). In some experiments we added brucite as a source of water.

144   Brucite breaks down to MgO and water at run conditions (e.g., Johnson and Walker, 1993)

145   and if the capsule remains closed, the breakdown products recombine to form brucite during

146   cooling because MgO is non-quenchable in the presence of water. We performed X-ray

147   diffraction of the powder from brucite present runs after annealing to ensure that the diffusion

148   data that we report are from runs with excess water (i.e. olivine is H saturated). **FIGURES 2**

149   **AND 3**

150 A final requirement to prevent breaking of the crystals was to use pressure and temperature

151 ramps (of ca. 30 minutes each) to start and end the experiments (e.g., Tingle, 1988). In

152 experiments carried out in this manner only few cracks formed in the crystals and those that

153 did form were perpendicular to the length of the cylinder so that the polished surface was still

154 available for analysis. However, such a slow cooling and decompression path combined with

155 the high diffusivity of H (Mackwell and Kohlstedt, 1990; Kohlstedt and Mackwell, 1998, and

156 1999; Demouchy and Mackwell, 2003 and 2006) allows it to leave the olivine crystals. Thus,

157 the measured water contents after annealing underestimates the actual concentration present in

158 the olivine during the runs. The magnitude of this degassing effect was established by

159 performing three additional experiments at 2 GPa and two selected temperatures (1200 and

160 1225 $^{\circ}$C). These runs were quenched in less than 1 minute to retain the H contents in olivines

161 from close to the annealing conditions. Inspection of these quickly quenched crystals with the

162 optical microscope shows that they contain numerous crystallographically oriented polyphasic

163 inclusions with bubble(s) and some unidentified transparent and opaque material (Fig. 4).

164 These inclusions were formed by the precipitation and nucleation of water during the fast

165 quench (Mackwell et al., 1985; Karato, 2006), because such inclusions were not seen in the

166 slowly quenched run products. During slow quench, excess H was able to escape from the

167 crystal by diffusion without precipitating inclusions. Although the crystals from the quickly

168 quenched runs cannot be used for the determination of diffusion coefficients (because as we

169 note above, they break into multiple pieces) we consider their OH concentrations to be

170 representative of those that prevailed in the crystals from which we obtained the diffusion

171 data. We have used a sequence of calculations to obtain the water contents at annealing

172 conditions, and based on that, fugacities of volatile species at run conditions for all crystals

173 (see section 3.3).

174 **FIGURE 4 AND TABLE 1**

175   Uncertainties related to the thermocouple calibration and pressure correction of the emf

176   reading are < 0.5 % (Mao et al., 1971). The main temperature uncertainty in piston cylinder

177   experiments is related to the presence of gradients in the furnace or the position of the

178   thermocouple and the crystals. Using the thermal analysis of Watson et al (2002) we estimate

179   that at our runs conditions and sample size (ca. 4 mm) temperature gradients are < 20 $^{\circ}$C, and

180   thus we have adopted a conservative temperature uncertainty of $\pm$ 10 $^{\circ}$C.

181

182   *2.3. SIMS analyses of olivine diffusion profiles*

183   After the anneals, single crystals were recovered and mounted in indium / epoxy for ion

184   microprobe analysis. Isotopic profiles were measured by secondary ion mass spectrometry

185   (SIMS) using a Cameca IMS 4f ion probe (University of Edinburgh, U.K.). A primary Cs-ion

186   beam (10 to 20 nA) was accelerated at 10 kV on to the Au-coated samples. High energy (300

187   ev) negative secondary ions were detected using an electron multiplier. The Si and O isotopes

188   were measured simultaneously (^{16}O, ^{18}O, ^{28}Si, ^{29}Si, ^{30}Si) and thus the position of the interface

189   could be inferred from profiles of both the elements, and diffusion rates of the two elements

190   could be studied in direct comparison. The depth of the profiles varied between 300 and 2700

191   nanometers and the sizes of the craters were about 100 x 100 μm. In total, 52 ion microprobe

192   isotope profiles have been obtained - 35 through annealed crystals and 17 in unannealed

193   crystals which were used for checking the composition and shapes of the diffusion couples

194   prior to experiments (i.e. initial conditions). Only 15 profiles have been finally used to obtain

195   diffusion coefficients, the rest being discarded due to problems mainly related to the

196   roughness of the sample surface. The lengths of the profiles were calibrated by measuring the

197   depths of the individual sputter pits using a profilometer. Typically, measurements were

198   carried out in four different directions for each crater and the crater morphology was also

199   inspected to avoid artefacts. The experimental setup discussed above allows two crystals to be

200 recovered from each run, allowing two determinations of diffusion coefficients from each

201 experiment. The convolution lengths (i.e., length of the transition zones) of unannealed

202 crystals range from 10 nm to 45 nm, whereas the lengths of the diffusion zones of the

203 annealed crystals ranged from about 200 to 700 nm. This means that convolution effects were

204 minimal, with a maximum possible 10 % overestimation of the diffusion coefficients

205 (Ganguly et al., 1988).

206

207 *2.4. Fourier Transform Infrared analysis of olivine*

208 After the anneal and in some cases after the ion microprobe analyses the crystals were

209 doubly polished and OH contents were determined by Fourier Transform Infrared

210 spectroscopy (FTIR). The spectra were obtained from oriented crystals and a polarized beam

211 of ca. 100 µm in diameter at the Bayerisches Geoinstitut (Germany) with a Bruker IFS 120

212 high-resolution FTIR spectrometer. Spectra were obtained in two perpendicular directions

213 (parallel to the *a* and *b* axes) for each crystal. A tungsten light source, a Si-coated CaF_2 beam

214 splitter and a narrow-band MCT detector were used for all measurements. Polarized

215 measurements were carried out with an Al wire strip polarizor on a KRS-5 substrate. During

216 the measurements, the interferometer chamber was kept under vacuum while the microscope

217 was purged with purified air. Two hundred scans were measured at 4 cm^{-1} resolution. The

218 spot size analyzed was determined by an aperture in the rear focal plane of the 15 fold

219 Cassegranian objective.

220

221 **3. H loss, interpretation of FTIR spectra, and fH$_2$O and fO$_2$ of the experiments**

222 Understanding the effect of water on ionic diffusion rates and mechanism depends

223 critically on our ability to determine the water fugacity of the experimental runs, and possibly

224 also the oxygen fugacity. This is not straightforward because the fH$_2$O and fO$_2$ cannot be

10

225   directly controlled in high P-T anneals in piston cylinder experiments. Constraining fH$_2$O and

226   fO$_2$ typically requires thermodynamic calculations combined with H determinations after

227   anneals. In this section we address in some detail the problem of H loss during quench, the

228   interpretation of the FTIR spectra of olivine, and how we obtain the volatile fugacities

229   ambient during the anneals.

230

231   *3.1. The case of H loss during quenching*

232   We have explored the extent of H loss from the olivines during quenching of the anneals

233   by a series of numerical experiments. The temperature-pressure-time (T-P-t) paths of

234   experiments were recorded by the computer which controls the piston cylinder experimental

235   apparatus. One dimensional diffusion calculations were carried out to model diffusion along

236   these T-P-t paths, and the results show that (Fig .5) already during the first 5 minutes of

237   decompression and cooling as much as 50 % of H is lost. This is similar to the difference

238   between the water contents of olivines from slowly and fast quenched runs, and suggests that

239   the low H content of olivines in the slowly quenched runs are due to diffusional H loss; these

240   samples were not annealed with such low H contents.

241   **FIGURE 5**

242   *3.2. FTIR spectra of olivines in the region 3100 to 3800 cm^{-1} and quantification of H$_2$O*

243   *concentration*

244   The FTIR spectra of the olivines were obtained with the incident light along the [001]

245   direction of olivine (Pbnm space group). The water contents that we report include the results

246   from spectra with the electric vector parallel to the [100] and [010] directions and follow the

247   approaches and calibrations described in Paterson (1982) and Bell et al. (2003). We did not

248   acquire FTIR spectra with the electric vector parallel to the [001] direction and thus the water

249   contents that we report are lower than the actual values. However, the contribution to the total

11

250   water content from that direction is relatively minor in many cases (e.g., Bell et al., 2003), and

251   is certainly < 30 % relative. Comparison between the water contents obtained using the

252   Paterson (1982) and Bell et al. (2003) calibrations showed that the latter gave concentrations

253   which are factors of 2.1 to 2.4 higher, similar to the value of 2.3 found by Bell et al. (2003).

254   Using the Bell et al. (2003) calibration, the highest water content we obtain is 370 ppm H_2O

255   from a brucite-present run at 2 GPa and 1225 ^{o}C that was rapidly quenched. This is ~ 20 %

256   lower than the value of 460 ppm H_2O at water saturation obtained for the same P, T and

257   forsterite content with the solubility model of Zhao et al (2004). This is an expected result

258   because the fluid in our runs was not pure water and contained significant amounts of other C-

259   H-O species (see below). The water content in olivines from brucite-absent runs (at 2 GPa and

260   1225 ^{o}C) that were quenched fast is 43 ppm. The crystals from slowly quenched runs have

261   low H_2O varying from ~ 7 to 30 ppm.

262   FTIR spectra of olivines obtained with the electric vector parallel to the [100] direction

263   show prominent peaks at 3612, 3600, 3579, 3573, 3544, 3527, and 3490-80 cm^{-1} (Fig. 6).

264   Measurements obtained parallel to the [010] direction show much lower absorbance and less

265   well defined peaks, some only show a bump between 3600 and 3500 cm^{-1}, and others have

266   peaks at 3612, 3546 (the most common one), 3525, and 3480 cm^{-1}. No significant peak was

267   found between 3100 and 3400 cm^{-1}. This might result from our measurements not being

268   parallel to the *c* axis (e.g., Lemaire et al., 2004), although FTIR spectra of unoriented crystals

269   annealed without brucite did not show any significant peak at these wavelengths either. There

270   is a positive correlation between the calculated water content and the relative peak intensities

271   for spectra parallel to the *a* axis. In particular, the size of the peaks at 3612 and 3600 cm^{-1}

272   decrease with decreasing water contents to the point where in one sample with very low water

273   (8 ppm) they are absent. A new peak is present at ca. 3527 cm^{-1}, and the peak at ca. 3579 cm^{-1}

274   decreases and shifts to 3571 cm^{-1}. A decrease in the bands at 3612 cm^{-1} and 3600 cm^{-1} was

275   also observed in the experiments of Mosenfelder et al. (2006), but the bands at 3527 cm^{-1} and

276   ca. 3579 cm^{-1} were absent in their study. The samples we annealed without brucite with

277   intermediate water contents (ca. 45 ppm H_2O) have spectra similar to that obtained from

278   natural olivines (e.g., Miller et al., 1987).

279   The interpretation of the FTIR spectra and OH vibrations in terms of H in a given position

280   of the olivine structure is a matter of intense research and interpretations (see Keppler and

281   Bolfan-Casanova, 2006). Aside from possible effects of the relative orientation of the crystal

282   and incident beam (e.g., Libowitzky and Rossman, 1996; Lemaire et al., 2004; our Fig. 6), the

283   temperature, pressure (e.g., Kohlstedt et al., 1996; Zhao et al., 2004; Mosenfelder et al.,

284   2006), oxygen fugacity (Bai and Kohlstedt, 1993), silica activity (Bai and Kohlstedt, 1993;

285   Matveev et al., 2001; Lemaire et al., 2004), and the major and trace element composition of

286   olivine (e.g., Zhao et al., 2004; Berry et al., 2005; Hauri et al., 2006), have been shown to

287   influence the solubility and FTIR spectra of OH in olivine. The data we report seem to

288   indicate spectral features may change as a function of total water content as well.

289   FTIR spectra of olivine has typically been interpreted considering two main possibilities:

290   the hydrogen is associated with vacancies (Si) or point defects in the tetrahedral site in which

291   case most peaks are at high wave numbers (e.g., 3650 to 3450 cm^{-1}; Group I bands of Bai and

292   Kohlstedt, 1993), or/and the H is associated with vacancies (e.g., Mg) or point defects (e.g.,

293   Fe^{3+}) in the octahedral site and the wave numbers are typically much lower (3450 to 3100 cm^{-1};

294   Group II bands of Bai and Kohlstedt, 1993). Ion microprobe measurement of H and other

295   trace elements in olivine annealed at water undersaturated conditions suggest a coupled

296   substitution with H and Al replacing Si, whereas at water saturation the H incorporation

297   mechanism changes to 2H for Mg (Hauri et al., 2006). If H is dissolved in olivine by

298   substituting for Mg only (an issue that is not completely settled yet, e.g., see Koch-Müller et

13

299 al., 2006), it needs to be clarified how Si diffusion rates are influenced by H. This is a

300 question that we return to in the discussion section. **FIGURE 6**

301

302 *3.3. Fluid composition and calculation of water and oxygen fugacities*

303   We obtained the ambient water and other volatile fugacities for the experimental runs in

304 several steps. First we use the water solubility equations of Zhao et al. (2004) to obtain the

305 fH_2O from the measured OH concentration in the olivine for the quickly quenched runs only.

306 For the brucite-absent runs the fH_2O is about 0.94 GPa, and it is about 9.4 GPa when brucite

307 was present. In a second step the fluid composition in the C-O-H system and the fugacities of

308 H_2O, CO_2, CO, CH_4, H_2, and O_2 were calculated using the fH_2O obtained above and the

309 constraint that graphite was present (i.e. activity of graphite = 1). The procedure has been

310 described in Holloway (1987). We used a modified Redlich-Kwong equation of state (EOS)

311 for fluids with the parameters from Holloway (1981) and considered ideal mixing. The

312 equilibrium constants of the species forming reactions were obtained from Robie and

313 Hemingway (1995) and the volumetric data of graphite from Holland and Powell (1998).

314 Mixing of thermodynamic data sources was necessary because there is no single internally

315 consistent database that contains all the data we needed. The fluid composition and fugacities

316 that we have calculated overlap with those obtained using the Perplex thermodynamic

317 algorithm (Connolly, 1990). Next, the ambient volatile fugacities of the slowly quenched runs

318 were calculated using the same procedure but with the assumption that the fluid composition

319 in these runs was the same as that obtained for the quickly quenched ones. Finally, we used

320 the calculated fH_2O and the water solubility model of Zhao et al. (2004) to obtain the

321 concentration of OH in olivine at anneal conditions for these slowly quenched runs. The

322 calculated water contents are 50% or more higher than the measured ones (Table 1) which is

323 consistent with the results of the cooling and decompression diffusion model explained above

14

324   (e.g., Fig. 5). The $f\text{H}_2\text{O}$ in the brucite-absent runs varies from 0.97 to 0.89 GPa (or 35 to 51

325   ppm H_2O in olivine) and $f\text{O}_2$ varies from $10^{-7.1}$ to $10^{-5.8}$ Pa (close to the iron-wüstite oxygen

326   fugacity buffer; Table 1) depending on temperature. For the brucite present experiments (all at

327   1200-1225 $^\text{o}$C) the volatile fugacities are higher, with $f\text{H}_2\text{O} \sim 9.4$ GPa (or 370 ppm H_2O in

328   olivine) and $f\text{O}_2 \sim 10^{-3.9}$ Pa, which is close to the fayalite-magnetite-quartz oxygen fugacity

329   buffer.

330

331   **4. Diffusion rates of Si and O in water-bearing olivine**

332   A finite difference algorithm was used to solve the diffusion equation and diffusion

333   coefficients (D) were obtained by simulating best fits to the observed isotopic profiles (Fig. 7;

334   Table 1). We considered two media (crystal plus thin film) which were allowed to have

335   different diffusivities; the thin film typically yielded higher values than the crystal. The

336   position of the crystal-film interface was initially set to be the same as that of the unannealed

337   sample that was coated and analyzed in the same batch as the sample used in the diffusion

338   anneal. The difference between the position of the interface obtained finally from that of the

339   unannealed sample were < 100 nm and probably reflects the variability within or between thin

340   film deposition sessions. The error of estimation of the diffusion coefficients varies, and

341   depends on the thickness of the thin film, length of the profile, and spatial resolution of the

342   ion microprobe session. Comparison between the results of different fits and between two

343   different crystals from the same run shows variations of 0.1 to 0.2 log units and thus we have

344   adopted errors on the diffusion coefficients of ± 0.15 log units.

345   A plot of lnD $vs.$ the inverse of temperature revealed a linear relation between the two and

346   a least-squares routine yielded the pre-exponential factor (D_o) and the activation energy (E^P)

347   from the relation:

348     $$D = D_o \cdot \exp\left(-\frac{E^P}{RT}\right)$$ (1)

349

350   where R is the gas constant. E^P can be expanded into $E^P = E^1 + (P-10^5)\,\Delta V$, where E^P is the

351   activation energy at pressure P in Pascals, E^1 is the activation energy at atmospheric pressure,

352   and ΔV is the activation volume. Using the data from the brucite-absent runs, we obtained: for

353   Si, $D_o = 1.68\ (\pm 3.52) \cdot 10^{-7}\ m^2 s^{-1}$ and $E^P = 358 \pm 28\ kJmol^{-1}$ (Fig. 8), and for O, $D_o = 1.43$

354     $(\pm 1.80) \cdot 10^{-4}\ m^2 s^{-1}$ and $E^P = 437 \pm 17\ kJmol^{-1}$ (Fig. 9). The Arrhenius parameters were

355   determined by least-squares linear fits to the data and we report uncertainties at the 1 sigma

356   level. The error on the activation energy reflect the scatter of the data which is typically larger

357   that the estimated errors on individual measurements of D and T. A full error propagation

358   analysis showed that incorporation of the errors on T and D quoted above changed the error

359   on the pre exponential factor by less than 5 %. Although we do not have enough Si data to

360   define the Arrhenius parameters for the runs annealed with $fH_2O = 9.4$ GPa, all data are

361   consistent with the same activation energy (Fig. 8). Unfortunately no O diffusion data was

362   retrieved at brucite-present runs because the diffusion profiles were too close to complete

363   equilibration. Moreover, there is no significant difference between the diffusion coefficients

364   measured along [001] and those obtained along [100] or [010], implying that there is no major

365   diffusion anisotropy in D_{Si} or D_O under water bearing conditions (Table 1). The O diffusion

366   rate is about a half an order of magnitude faster than that of Si at high temperature (e.g., 1350

367   ^{o}C) but both rates overlap at 1150 ^{o}C. At lower temperatures, whether D_{Si} is indeed greater

368   than D_O or this is an artefact of the scatter of our data remains to be verified by direct

369   experiments at temperatures below 1150 °C. It is worth noting that this analysis of the data

370   yields 'apparent' activation energies because it is not possible to vary T, fO_2 and fH_2O

371   independently in high pressure experiments, and our study is no exception. A change in

372   annealing temperature also corresponds to a change in the $f\mathrm{O}_2$ and $f\mathrm{H}_2\mathrm{O}$ (Table 1) (see also

373   Ganguly et al., 1998; Holzapfel et al., 2007). Thus, the E^{P} we have determined reflects the

374   temperature dependence but also incorporates the effects due to variation of $f\mathrm{O}_2$ and $f\mathrm{H}_2\mathrm{O}$

375   with temperature, and these need to disentangled. .**FIGURES 7, 8 AND 9**

376

377   *4.1. Effect of variation of fH_2O, fO_2 and $aSiO_2$ in the experiments on the retrieved values of*

378   *D_o and E^P*

379   The variables that completely describe the system that we are dealing with (olivine plus

380   fluid) can be determined by the Gibbs phase rule. In the water bearing case, there are 5

381   components (O, Si, Mg, Fe, H), and 5 or 6 degrees of freedom (e.g., T, P, Fe/Mg, $f\mathrm{O}_2$, $a\mathrm{SiO}_2$,

382   and $f\mathrm{H}_2\mathrm{O}$) depending on whether the system is fluid saturated or not. We maintain constant P,

383   T and Fe/Mg in our experiments but we also need to consider $f\mathrm{O}_2$, $f\mathrm{H}_2\mathrm{O}$, and $a\mathrm{SiO}_2$. These

384   variables can be incorporated into the diffusion or deformation constitutive laws through

385   exponentials (e.g., Misener, 1974), but most experimental results suggest that it is best to

386   incorporate them in the pre-exponential factor D_o (e.g., Hirth and Kohlstedt, 2003; Dohmen

387   and Chakraborty, 2007). This is the form of dependence that we will consider for the

388   subsequent analysis, i.e.:

389

390     $D_o = A \bullet f\mathrm{O}_2{}^n \bullet f\mathrm{H}_2\mathrm{O}^r \bullet a\mathrm{SiO}_2{}^m$ (2)

391

392   where A is a constant, $a\mathrm{SiO}_2$ is the silica activity, and n, r and m are the exponents of the

393   independent variables.

394   The variation of $f\mathrm{H}_2\mathrm{O}$ in the experiments used to determine D_o and E^{P} is relatively small -

395   from 0.89 to 0.97 GPa (Table 1). If we assume for a moment that the $f\mathrm{H}_2\mathrm{O}$ exponent r takes

396   values of 1 or even 2 (e.g., Kohlstedt and Mackwell, 1998; Mei and Kohlstedt, 2000), D_{Si} or

397   D_O change by a maximum factor of 1.2 over the experimental conditions of our study and thus

398   would have a limited effect on the values of kinetic parameters that we report. This implies

399   that the activation energies for O and Si diffusion that we derive are effectively for a constant

400   fH_2O of ca. 0.93 (±0.04) GPa.

401   The effect of the $aSiO_2$ is difficult to address since this parameter has not been directly

402   controlled in our experiments. Dohmen et al. (2007) reported excess silica in olivine thin

403   films deposited with the same laser conditions that we have used to produce our thin films,

404   and thus it is likely that the activity of silica was buffered by the coexistence of silica with

405   olivine and orthopyroxene. The same $aSiO2$ would be imposed by the talc of the pressure cell

406   assembly because it breaks down to enstatite, α-quartz and water vapour at the experimental

407   P, T conditions (e.g., Pawley and Wood, 1995; Bose and Ganguly, 1995b). Therefore, if we

408   assume that the coexistence of enstatite and olivine defined the silica activity in our runs, then

409   the temperature dependence of that reaction would provide us a measure of the difference in

410   silica activity between the highest and lowest temperature runs of our study. The temperature

411   dependence of silica activity for the enstatite-forsterite reaction is less than a factor of 1.05 for

412   a change between 1200 ^{o}C and 1350 ^{o}C at 2 GPa (e.g., Ghiorso and Carmichael, 1987). This

413   factor, when combined with the maximum expected exponent of m = 4 for many charge

414   neutrality conditions under dry or wet conditions (e.g., Kohlstedt and Mackwell, 1998),

415   suggests that the D values would be affected by a maximum factor of 1.2. This indicates again

416   that the kinetic parameters for the brucite-absent runs that we report are basically derived at a

417   constant $aSiO_2$. The silica activity of the brucite-present runs could have been lower than the

418   brucite-absent and water-poor runs, with the possibility that it was controlled by the

419   coexistence of periclase, silica and forsterite. However, whether this reaction can impose the

420   silica activity in the diffusion zone depends on its ability to overwhelm the excess silica of the

421   thin film (Dohmen et al., 2007).

422   This relatively limited variation of $f\mathrm{H_2O}$ and $a\mathrm{SiO_2}$ due to change in temperature of our

423   experiments contrasts with a variation of about a factor of 25 in $f\mathrm{O_2}$ within the investigated T

424   range ($f\mathrm{O_2}$ varies from $6.3 \cdot 10^{-8}$ Pa to $1.6 \cdot 10^{-6}$ Pa). Gérard and Jaoul (1989) and Ryerson et al.

425   (1989) reported positive exponents that vary between 1/3 and 1/5 (determined at atmospheric

426   pressure and dry conditions) for the dependence of D_O on $f\mathrm{O_2}$. If we normalize the dry data of

427   Gérard and Jaoul (1989), Ryerson et al. (1989), and Dohmen et al. (2002b) to the $f\mathrm{O_2}$ of our

428   experiments, we find that (i) the activation energies obtained from the dry and wet

429   experiments overlap (Table 2), and (ii) if the exponent n is assumed to be the same at wet and

430   dry conditions, then the activation energy at constant $f\mathrm{O_2}$, high pressures and wet conditions

431   lies between 290 and 350 kJmol^{-1} (Fig. 10). It is interesting to note that from computer

432   simulations it has been proposed that there is no change in the diffusion mechanism of O in

433   pure forsterite between water bearing and dry conditions (Walker et al., 2003). For Si

434   diffusion, Houlier et al. (1990) reported a negative dependence of the Si diffusion rate on $f\mathrm{O_2}$

435   under dry 1 atmosphere conditions and this would lead to activation energy at constant $f\mathrm{O_2}$, at

436   high pressures and wet conditions of 450 kJmol^{-1} for Si. However, the data of Houlier et al.

437   (1990) are rather scattered and could also be fitted without any dependency on $f\mathrm{O_2}$, which is

438   in agreement with unpublished experimental results from our laboratory (R. Dohmen,

439   personal communication). This implies that the activation energy for Si diffusion obtained by

440   fitting the raw data remains unchanged when the effects of variation of $a\mathrm{SiO_2}$, $f\mathrm{H_2O}$ and $f\mathrm{O_2}$

441   with the experimental run temperatures are accounted for.

442   **FIGURE 10 AND TABLE 2**

443   **5. Si and O diffusion: the effect of water and pressure**

444   The effect of water on diffusion rates can be quantified by comparing two datasets (dry and

445   wet, or two different water fugacities) measured at constant values of the remaining variables

446   (i.e., P, T, Fe/Mg, $f\mathrm{O_2}$ and $a\mathrm{SiO_2}$). This can be readily done by comparing the diffusion

19

447 coefficients of Si obtained from our brucite-present and brucite-absent experiments at 1200

448 ^{o}C. We find that the Si diffusion rate increases on average by a factor of ~ 2 for an increase of

449 a factor of ~10 in fH$_2$O (from 0.97 to 9.4 GPa). Although this average value would imply $r =$

450 1/3 in Eqn.2, the scatter of the data permits r to lie between 1/5 and 1 (see below). D$_{Si}$ at fH$_2$O

451 of *ca.* 0.93 GPa is about 2000 times, and D$_O$ about 10 to 70 times, faster (at 1200 ^{o}C) than

452 those at 1 atmosphere and dry conditions (see Table 2), if the pressure effect is ignored as a

453 first approximation. Thus, taken on face value, these data indicate a large effect of water on Si

454 diffusion and a smaller effect on O diffusion.

455

456 *5.1. Analysis of the relation between water fugacity and transport properties*

457   A diffusion coefficient (D^w) in a water bearing system is given by

458     $$D^w = A^w \cdot f_{O_2}{}^{nw} \cdot f_{H_2O}{}^{r} \cdot a_{SiO_2}{}^{mw} \cdot \exp\left(-\frac{E^{1w} + (P - 10^5)\,\Delta V^w}{RT}\right) \qquad (3),$$

459   where the letter w in the superscripts indicates "water bearing". For a set of data where

460 everything other than water fugacity (fH$_2$O) is held constant, one obtains

461     $\ln D^w = A' + r \ln f$H$_2$O $\qquad$ (4),

462

463   with A' = ln (A^w • $f_{O2}{}^{mw}$ • $a_{SiO2}{}^{mw}$) + (-E^{Pw}/RT), using E^{Pw} = E^{1w} + (P-10^5)ΔV^w.

464   Analogously, for dry conditions, one can write

465     $$D^d = B^d \cdot f_{O_2}{}^{nd} \cdot a_{SiO_2}{}^{md} \cdot \mathrm{Exp}\left(-\frac{E^{1d} + (P - 10^5)\,\Delta V^d}{RT}\right) \qquad (5)$$

466   for diffusion in olivine of a given composition, where the superscript "d" stands for dry.

467 This can be reduced to

468

469     $\ln D^d = B' + B''\,\Delta V^d$, $\qquad\qquad\qquad$ (6)

20

470

471   with B' = ln ($B^d \cdot f_{O2}{}^{nd} \cdot a_{SiO2}{}^{md}$) + ($-E^{1d}/RT$), and B" = [$-(P-10^5)/RT$].

472

473   Eqns. (3) - (6) allow the wet to dry transition to be explored in a number of ways (Fig. 11).

474   First, wet data from two different water fugacities may be used to obtain r, as the slope of a

475   line on a plot of ln D^w vs. ln fH$_2$O (e.g. for Si diffusion data in this study). Secondly, values of

476   r obtained from independent constraints (e.g. point defect models) may be used to explore the

477   likely variation of a diffusion coefficient with water fugacity (e.g. for O diffusion data, see

478   below). Thirdly, Eqns. (4) and (6) may be equated to obtain the condition for transition from

479   "dry" to "wet" behavior as a function of P, T etc.:

480

481   A' + r ln fH$_2$O* = B' + B" ΔV^d ,

482

483   where fH$_2$O* is the value of fH$_2$O at which the transition occurs. fH$_2$O* can be determined if

484   the values of r and ΔV^d are known. More usefully, the poorly constrained variables r and ΔV^d

485   can be varied within reasonable limits to obtain a plausible range for the very important

486   parameter fH$_2$O* for a number of physical properties. Note that this analysis considers the wet

487   to dry transition to occur as a kink at a point, fH$_2$O*, whereas in practice the transition may be

488   smeared continuously over a range of fH$_2$O values centered about fH$_2$O*. Equations similar to

489   (3) - (6) can be written for diffusion of other species (e.g. Fe-Mg), deformation and electrical

490   conductivity (e.g. see Hirth and Kohlstedt, 2003; Hier-Majumder et al., 2005; Karato, 2006).

491   For dislocation creep, a related form of the equation is used (e.g. Hirth and Kohlstedt, 2003):

492     $$\dot{\varepsilon} = A_{def} \cdot \sigma^{ne} \cdot f_{H_2O}{}^{r} \cdot Exp\left(-\frac{E^1 + P\,\Delta V}{RT} \right) \qquad (7)$$

493 Here, $\dot{\varepsilon}$ = strain rate, A_{def} is a constant that includes the effects of fO_2 and $aSiO_2$, σ is

494 differential stress, 'ne' is the differential stress exponent (= 3.5 ± 0.3; Hirth and Kohlstedt,

495 2003), and the rest of the symbols have the usual meanings. As above, the various exponents

496 and activation parameters have different values for "wet" and "dry" dislocation creep.

497 **FIGURE 11**

498 *5.2. Diffusion of silicon and oxygen*

499 The activation volume for Si diffusion under dry conditions determined between 4 and 9

500 GPa and at 1490 ^{o}C was found to be around zero, $\Delta V^d_{D_{Si}} = 0.7 (\pm 2.3) \cdot 10^{-6}$ m^{3}mol^{-1} (Béjina

501 et al., 1999). The only other activation volume determined for diffusion in olivine at dry

502 conditions is that of Fe-Mg, which varies between 4 and 7 $\cdot$ 10^{-6} m^{3}mol^{-1} (Misener, 1974;

503 Farber et al., 2000; Holzapfel et al., 2007), and a value for $\Delta V^d_{D_{Fe-Mg}}$ of 7 $\cdot$ 10^{-6} m^{3}mol^{-1} was

504 determined for a constant fO_2 (see discussion in Holzapfel et al., 2007). Note that this value is

505 significantly smaller than the wet activation volume for the diffusion of the same elements,

506 $\Delta V^w_{D_{Fe-Mg}}$ of 16 (± 6) $\cdot$ 10^{-6} m^{3}mol^{-1} (Hier-Majumder et al., 2005). Karato (2006) suggests,

507 based on a model of homologous temperature scaling or elastic strain energy, that the

508 activation volume for Si diffusion in olivine should be similar to that for Mg-Fe diffusion. We

509 will therefore consider two extreme values for $\Delta V^d_{D_{Si}}$ - an activation volume of zero and one

510 equal to that of Fe-Mg at a constant fO_2 (for dry conditions). A plot of log fH_2O *vs.* log D of

511 the water bearing and dry data together with lines for the exponent, *r*, of 2, 1, 0.5 and 0.2 is

512 shown in Figure 12. Combining these observations with constraints from point defect

513 thermodynamics and charge neutrality conditions that have been considered in the literature

514 (see below), we find that values of *r* between 0.5 and 1 are most likely. With the permissible

515 limiting exponents of 0.2 and 1, the values of log fH_2O^* vary between ca. -10 and 6.2 Pa,

516 corresponding to < 0.1 ppm H_2O in the olivine (Table 3) if the water solubility model of Zhao

22

517   et al. (2004) is used. Varying the values of $\Delta V^d_{D_{Si}}$ down to zero or changing T by $\pm$ 100 ^{o}C to

518   explore uncertainties does not alter the observation that the wet to dry transition occurs at < 5

519   ppm H_2O in the olivine (Table 3). These water contents are even lower than those measured in

520   many olivine crystals from mantle xenoliths (e.g., Bell and Rossman, 1992) at the surface.

521   The implication is that to properly model the Si diffusion rates in the mantle we need to use

522   the water-bearing rather than dry kinetic parameters.

523   To analyse the effect of water on the diffusivity of oxygen, we need to consider in addition

524   that this diffusivity depends on fO_2. We have normalized the dry diffusion data to the same

525   fO_2 as that of our experiments (fO_2 = 6.3 *10^{-8} Pa) using the exponent, n, of 1/3 (Gérard and

526   Jaoul, 1989), 1/5 (Ryerson et al., 1989), or an intermediate value of 1/4 (Dohmen et al.,

527   2002b). The activation volume for D_O under dry conditions is unknown and so we have varied

528    $\Delta V^d_{D_O}$ from zero to 7 • 10^{-6} m^3mol^{-1} following the data and approach for Fe-Mg and Si noted

529   above (Fig. 12 and Table 3). For the same ranges of water fugacity exponents (r = 2, 1, 1/2,

530   and 1/5) the log fH_2O* values for O are in general higher than those of Si, varying from about

531   8.2 to ca. 1 Pa. Nonetheless, they also correspond to water contents in olivine of < 0.1 to 10

532   ppm H_2O. Changing the fO_2 dependence of O diffusivity has a limited effect on the log fH_2O^*

533   values (not shown). Thus, for O diffusion as well we can conclude that "wet" diffusion laws

534   apply to most mantle olivines. **FIGURE 12 AND TABLE 3**

535   The data we have for Si diffusion suggests an r exponent between 0.5 and 1 whereas no

536   quantitative constraint can be derived for this exponent for O. We have calculated the kinetic

537   parameters for Si diffusion incorporating explicitly the effect of water (Eqn. 2) and using the

538   mean value of fH_2O (= 0.93 GPa) from our experiments:

539        $$D^w_{Si}(m^2s^{-1}) = \cdot \alpha^w_{Si}(m^2s^{-1}Pa^{-1}) \cdot f_{H_2O}{}^r \cdot (Pa) \cdot \exp\left(-\frac{358\,(kJmol^{-1}) \pm 28}{RT}\right).$$

540   Here, if $r = 1$, α_{Si}^{w} is $1.8 \cdot 10^{-16}$ and if $r = 0.5$, α_{Si}^{w} is $5.5 \cdot 10^{-12}$. This equation is only valid for

541    $\log fH_2O$ (fH_2O in Pa) values higher than about 6.

542

6. Inferences from point defects models and Si and O diffusion mechanisms

544   The mechanisms of Si and O diffusion in olivine can be addressed by considering the point

545   defect chemistry of olivine (Smyth and Stocker, 1975; Stocker and Smyth, 1978; Nakamura

546   and Schmalzried, 1983; Hobbs, 1984; Kohlstedt and Mackwell, 1998, and 1999; Tsai and

547   Dieckmann, 2002; Kohlstedt, 2006; Dohmen and Chakraborty, 2007). We use the Kröger-

548   Vink (1965) notation, e.g. V''_{Me} indicates two effective negative charges for a vacancy in the

549   octahedral metal site, whereas $Fe^{\bullet}_{Me}$ indicates an effective charge of $+1$ for a Fe^{3+} on the Me

550   site. Square brackets [..] denote concentration of the corresponding units.

551   Water derived point defects can be 'isolated', such as $(OH^{\bullet})_O$, or associated with other

552   defects such as vacancies on the Me or Si sites, or with aliovalent impurities substituting in

553   regular sites (e.g., Kurosawa et al., 1997; Brodholt and Refson, 2000; Braithwaite et al., 2003;

554   Karato, 2006; Kohlstedt, 2006). Based on earlier studies, it has been considered likely that the

555   relevant "water defect" is $\{2(OH^{\bullet})_O - V''_{Me}\}^{x}$. The main reason for this preference (Kohlstedt,

556   2006) is that it leads to a water fugacity exponent of ~ 1, which is the value found in water

557   solubility (Kohlstedt et al., 1996) and Fe-Mg diffusion (Hier-Majumder et al., 2005)

558   experiments. Thus, the vacancy concentration in the Me site would control the amount of

559   water incorporated in olivine (Kohlstedt, 2006). A key parameter for establishing a point

560   defect model is the charge neutrality condition. We have compiled (Table 4) the water

561   fugacity exponents associated with the most likely charge neutrality conditions and the

562   different point defects in olivine. Our diffusion data allows us to eliminate a subset of these

563   possibilities at the outset. Since the diffusion rates of Si and O *both* increase with fH_2O, the r

564   exponents for both elements need to be positive and only these cases need be considered

565   further. Irrespective of further assumptions and uncertainties, this implies that the diffusion

566   mechanisms of the two elements (Si and O) in water bearing olivine would have to be

567   different (Table 4).

568   Consideration of our experimental observation that r for Si diffusion lies between 0.2 and 1

569   allows the choice of point defect models and diffusion mechanisms to be narrowed further

570   down to two options only (see Table 4): (1) Charge neutrality condition $[Fe^{\bullet}_{Me}] = [\{(OH^{\bullet})_O -$

571    $V''_{Me}\}']$, implying $r = 1$ for Si with interstitial diffusion or $r = 1/2$ involving Si-vacancy

572   associates, and $r = 1/2$ for O diffusing by a vacancy mechanism, or, (2) the charge neutrality

573   condition $[(OH^{\bullet})_O] = 2\ [V''_{Me}]$, with $r = 2/3$ for Si diffusing by a vacancy or $r = 1$ via the

574   associated complex $\{(OH^{\bullet})_O - V''''_{Si}\}'''$, and $r = 1/3$ for oxygen diffusing by an interstitial

575   mechanism. To unequivocally resolve which of these two options apply to diffusion processes

576   in hydrous olivine it is necessary to obtain additional experimental data. For example,

577   determination of the fO_2 dependence of O diffusion rates in olivine under water-present

578   conditions would help to clarify the situation (the exponent, nw, would be positive or negative

579   depending on the diffusion mechanism, see Kohlstedt and Mackwell, 1999; Karato 2006 for

580   further details). However, based on the available observations so far it appears that the second

581   option involving Si-vacancy or vacancy associates, $\{(OH^{\bullet})_O - V''''_{Si}\}'''$, may be the relevant

582   mechanism for Si diffusion. The line of reasoning is as follows: (i) Computer simulations of

583   Walker et al. (2003) indicate that water incorporation does not alter the diffusion mechanism

584   of O in forsterite, (ii) we find that the activation energies of O diffusion in mantle olivine at

585   dry and wet conditions are very similar. If (i) and (ii) are used to infer that the mechanism of

586   diffusion of O is the same (Note: this does not imply that the *rates* are the same) under wet

587   and dry conditions, then (iii) we can use the observed mechanism of diffusion of O under dry

588   conditions to infer the mechanism of diffusion under wet conditions. The positive correlation

589   between D_O and fO_2 (Gérard and Jaoul, 1989; Ryerson et al., 1989) suggests that oxygen

590 diffuses by an interstitial mechanism in dry conditions. If we accept this inference, then Si has

591 to diffuse by a different (see above), i.e. vacancy mechanism. This leads us to prefer the

592 second option above, involving Si-vacancy or vacancy associates, $\{(OH^{\bullet})_O - V''''_{Si}\}'''$. Note

593 that this diffusion mechanism leads to an exponent of 1 and therefore also agrees with the

594 observations of Kohlstedt (2006).

595 **TABLE 4**

596 *6. 1. Relation between Si diffusion, concentrations of vacancies, and water content*

597 The effect of H on Si diffusion rates via vacancies can be rationalized using the relation

598 between mobility and diffusion coefficients (e.g., Schmalzried, 1974; pages 53-55) which

599 leads to $D_{Si} = [V_{Si}] \bullet D_{V_{Si}}$, where V_{Si} includes all vacancy types on the silicon site, including

600 any of the associated complexes. This shows that faster diffusion of Si at wet conditions could

601 result from a higher number of vacancies, from a higher diffusion rate of the vacancies, or

602 both. The question that arises then is: how is it possible to increase the vacancy concentration

603 and diffusion coefficient of Si by such a large factor if the inferred charge neutrality

604 conditions indicate that H mainly goes into the Me sites? To address this question, we make

605 the assumption that diffusivities of vacancies in the olivine structure, whether they are on the

606 metal or the tetrahedral site, are of the same order of magnitude i.e. $D_{V_{Si}} \approx D_{V_{Me}}$. This is

607 consistent with inferences already made from various physical property measurements (e.g.,

608 Mackwell et al., 1988; Wanamaker, 1994; Kohlstedt, 2006). Then it follows that $D_{Si} = [V_{Si}]$

609 $\bullet D_{V_{Si}} \approx [V_{Si}] \bullet D_{V_{Me}} = [V_{Si}] \bullet (D_{Fe-Mg} / [V_{Me}])$, or, $[V_{Si}] = D_{Si} \bullet ([V_{Me}] / D_{Fe-Mg})$. Using this

610 relationship, we obtain $[V^d_{Si}] \approx 3 \bullet 10^{-12}$ using D_{Fe-Mg} from Dohmen and Chakraborty (2007),

611 D^d_{Si} from Dohmen et al. (2002b), and $[V^d_{Me}] \approx 9 \bullet 10^{-5}$ from Dohmen and Chakraborty, (2007)

612 (Table 5). Likewise, we obtain $[V^w_{Si}] \approx 6 \bullet 10^{-8}$ using D_{Fe-Mg} from Hier-Majumder et al. (2005),

613 D^w_{Si} from this study, and $[V^w_{Me}] \approx 4 \bullet 10^{-4}$ using the approach of Wang et al. (2004). The

26

614   interesting aspects are that (i) the vacancy concentrations are several orders of magnitude

615   smaller than the concentration of water dissolved in olivine, and (ii) the number of water

616   related defects in the Me-site, e.g., $[V_{Me}^w] \approx 4{\cdot}10^{-4}$ whereas $[V_{Si}^w] \approx 5{\cdot}10^{-8}$. This means that

617   only about 0.01 % of the H that enters the olivine structure might already substantially

618   enhance the Si vacancy concentrations (e.g. from $[V_{Si}^d] \approx 3{\cdot}10^{-12}$ to $[V_{Si}^w] \approx 5{\cdot}10^{-8}$) and

619   therefore, the Si diffusion and dislocation creep (depending on the precise role of oxygen not

620   considered here) rates. This analysis is also consistent with the observation that the wet to dry

621   transition for Si diffusion occurs at much lower water contents than for Fe-Mg diffusion (see

622   below).

623

624   **TABLE 5**

625   **7. The wet to dry transition for Fe-Mg diffusion and dislocation creep in olivine and**

626   **their relation to Si and O diffusion**

627   We now consider the experimental data on ionic diffusion and deformation under wet and

628   dry conditions to try to develop an integrated undertanding of how water enters the olivine

629   structure and affects these processes. The nature of influence of water on these processes is

630   embodied in the exponent r, the critical fH_2O* of transition from "wet" to "dry" laws (see

631   section 5.1) and in the activation energies and volumes. Similarity of these values for different

632   processes should point to similar underlying atomistic mechanisms (e.g., Karato, 2006;

633   Kohlstedt, 2006)

634

635   *7.1 Fe-Mg diffusion*

636   We find that the "wet" to "dry" transition for this process occurs at $\log fH_2O^* = 8.5$ (or about

637   11 ppm H_2O in the olivine) when Fe-Mg diffusion coefficients at 2 GPa, 1200 °C, $fO2 = 10^{-2.3}$

638   Pa (Ni-NiO buffer) and an olivine composition of Fo_{86} are compared (Fig. 13, wet data: Hier-

639 Majumder et al., 2005; dry data: Dohmen and Chakraborty, 2007). This transition point (log

640 fH$_2$O*) is about 3 log units higher than that for Si diffusion for almost the same exponent ($r =$

641 1) (Table 3) and represents the minimum water fugacity at which the "wet" equation for Fe-

642 Mg diffusion can be used. The enhancement of Fe-Mg diffusion rates from "dry" conditions

643 to a fH$_2$O = 0.93 GPa is only by a factor of two, compared to factors of 1000 and 50 for Si and

644 O diffusion, respectively. Note that this enhancement of Fe-Mg diffusion is smaller than that

645 reported by Hier-Majumder et al (2005) because they did not normalize the dry diffusion

646 coefficients to the oxygen fugacity of their experiments for comparison. The observations that

647 (i) the wet to dry transition for Fe-Mg diffusion occurs at higher water fugacities than for Si

648 and O diffusion and (ii) the effect of water on this diffusion rate is smaller than its effect on Si

649 and O diffusion are consistent with the point defect systematics we have discussed above

650 (Section 6.1).

651

652 *7.2 Dislocation creep*

653 We have carried out a similar comparison of dry and wet creep data for olivine using the

654 constitutive laws and parameters reported by Hirth and Kohlstedt (2003), considering the

655 uncertainties in activation volume (between 13 and 27 $\bullet 10^{-6}$ m^{3}mol^{-1}) and an exponent, r of

656 1.2 (Hirth and Kohlstedt, 2003; Fig. 13, Table 3). The transition point, log fH2O*, lies

657 between 6.1 and 7.0 (or, < 0.3 ppm water in olivine), which is similar to the value of ~ 7.6

658 found by Mei and Kohlstedt (2000) using slightly different data. This value is two orders of

659 magnitude below the transition point for Fe-Mg diffusion (Section 7.1) but is at the upper end

660 of the range of values found for Si diffusion (Table 3), with the same value for the exponent,

661 r, of 1. This points to a strong connection between the process of creep and diffusion of Si in

662 olivine (Fig. 13).

28

663   The connection can be evaluated further by considering the activation energies of different

664   processes. Dohmen et al. (2002b) and Kohlstedt (2006) argued that diffusion of Si controls

665   the creep of olivine under dry conditions because the activation energies of the two processes

666   are identical and Si is the slowest diffusing species in olivine at those conditions. In the

667   presence of H_2O, the rates of Si and O diffusion are more similar to each other and therefore it

668   is reasonable to expect that creep may be controlled by both processes. The activation

669   energies for the concerned processes in the presence of water are: 358 ± 28 kJmol^{-1} for Si

670   diffusion, 437 ± 17 kJmol^{-1} for O diffusion (this study) and 500 ± 40 kJmol^{-1} (Hirth and

671   Kohlstedt, 2003) or 410 ± 40 kJmol^{-1} (Karato, 2006) for creep. The activation energy for Si

672   diffusion is lower than that for creep, although there is a slight overlap with the value found

673   by Karato (2006) when errors are considered. On the other hand, the activation energy for O

674   diffusion is very similar to the value for creep found by Karato (2006) and overlaps within

675   error with the value obtained by Hirth and Kohlstedt (2003). Therefore, in water bearing

676   olivine where diffusion rates of Si and O are similar, creep rate appears to be controlled by an

677   interplay of Si and O diffusion. The exponent, r, for creep is close to that for Si diffusion and

678   the activation energy is closer to that for O diffusion.

679   In summary, we find that the wet to dry transition for various physical properties (Fe-Mg

680   diffusion, Si diffusion, O diffusion and creep) occurs at relatively low water fugacities and

681   water contents in olivine (< 10 ppm), even when all likely variation and uncertainties in

682   various parameters are considered (Table 3). Such water concentrations are lower or similar to

683   those measured in many mantle xenoliths or olivine xenocrysts (e.g. Bell and Rossman, 1992;

684   Ingrin and Skogby, 2000). Thus, it can be expected that the physical properties of the upper

685   mantle (viscosity, electrical conductivity, diffusion rates) will be affected by water even if the

686   mantle is largely water undersaturated. This implies that experimental studies that investigate

687   the effects of small amounts H on the physical and chemical properties of mantle materials are

29

688 directly relevant to understanding the rheological and chemical evolution of mantle; the effect

689 of H should be incorporated in numerical models of mantle dynamics (see section 8). This

690 finding is in agreement with studies that model the mantle flow under the western U.S.A. -

691 these seem to require a 'wet' rheological law (Dixon et al., 2004; Freed and Bürgmann, 2004).

692

693 **8. Calculating strain rates of water-bearing olivine from Si and O diffusion data**

694 The foregoing discussions suggest a close connection between the diffusion of Si and O

695 and dislocation creep of olivine. To quantitatively test this relation we have used our diffusion

696 data in three creep models (following Kohlstedt, 2006) to try to reproduce the experimentally

697 measured strain rates. In the model of Weertman (1999), most of the strain is produced by

698 glide and only a small fraction is produced by climb, but it is dislocation climb that controls

699 the strain rate which is given by:

700

701 $$\dot{\varepsilon} = 2\pi \cdot \frac{GV_m}{RT} \cdot (\frac{\sigma}{G})^3 \cdot \frac{D_{self}}{b^2} \cdot \frac{1}{\ln(G/\sigma)} \cdot \frac{\lambda_g}{\lambda_c}$$

702 where G = shear modulus, V_m = molar volume, b = Burgers vector, λ_g = glide distance, λ_c =

703 climb distance and D_{self} is the self-diffusivity. In the model of Nabarro (1967), with the

704 correction of a 2π factor due to Nix et al. (1971), all the strain is accomplished by climb and

705 one obtains:

706

707 $$\dot{\varepsilon} = 2 \cdot \frac{GV_m}{RT} \cdot (\frac{\sigma}{G})^3 \cdot \frac{D_{self}}{b^2} \cdot \frac{1}{\ln(4G/\pi\sigma)}$$

708

709 Finally, the model of Evans and Knowles (1978) also contains the Poisson's ratio (ν), and all

710 the strain is generated by glide but the creep rate is governed by climb, given by

711

712 $$\dot{\varepsilon} = \frac{4.2\sqrt{3}\,\pi}{\alpha^2} \cdot \frac{GV_m}{RT} \cdot (\frac{\sigma}{G})^3 \cdot \frac{D_{self}}{b^2} \cdot \frac{1}{\ln(\alpha G/2\sigma)} \cdot \{1 + \frac{2}{\alpha}[1 + \frac{1}{2\pi(1-\nu)}]\}\ ,$$

713

714   where $\alpha = 1.6$. All three equations contain the self-diffusion coefficient, which provides a

715   direct link between the strain rate and volume diffusion. Although D_{self} has a unique meaning

716   in the context of the original experimental data on pure metals that were used to obtain such

717   relations, in the case of olivine its meaning is more ambiguous. It probably relates to the flux

718   of the entire molecule of olivine and thus requires a multicomponent ($\tilde{\tilde{D}}$) formulation (Ruoff,

719   1965; Dimos et al., 1988; Jaoul 1990; Kohlstedt, 2006). Since $\tilde{\tilde{D}}$ is similar to the diffusivity

720   of the slowest ion, we have used the values of D_{Si} or D_O (depending on which is the slowest)

721   as a proxy for D_{self} to calculate the strain rates. **FIGURE 14**

722   It is apparent that the strain rates calculated with the Nabarro (1967) model are about one

723   order of magnitude lower than those obtained using the Evans and Knowles (1978) equation

724   and overlap with those from Weertman (1999) when $\lambda_g / \lambda_c = 0.1$ (Fig. 14). More

725   significantly, the strain rates calculated using the Nabarro (1967) formulation are about one to

726   two orders of magnitude smaller than those obtained from the flow law using the values of

727   Hirth and Kohlstedt (2003). The strain rates obtained using the expression from Evans and

728   Knowles (1977) agree with the flow law at low differential stress (10^4 to 10^5 Pa) but

729   underestimate them by about 1 order of magnitude at higher values of differential stress (10^7

730   to 10^8 Pa). The strain rates obtained using the equation from Weertman (1999) overlap with

731   the flow low values if λ_g/λ_c takes values between 1 and 10. We feel that the extent of

732   agreement between the strain rates calculated from diffusion data and those obtained from

733   experimentally determined flow laws is rather good, in particular for low strain rates ($< 10^5$

734   Pa) and for models where dislocation climb has an important role in limiting creep rates,

735   although glide causes much of the strain. The best fits are obtained if it is assumed that climb

736   and glide of dislocations contribute about equally to dislocation creep of olivine under

737   hydrous conditions. We would like to note here that the discrepancy in slope between strain

738   rates calculated from diffusion data and those obtained from fits of flow laws to experimental

739   data arise because the differential stress exponent for the models are close to 3 whereas that

740   for the experimental fit to flow laws is higher (about 3.5, Hirth and Kohlstedt, 2003) i.e. it is

741   intrinsic to the nature of the models.

742

743   **9. Conclusions**

744   Our experimental results show that even low amounts of H ($\sim$ 45 ppm H_2O in olivine) at

745   high pressure (2 GPa) considerably enhance the diffusion rates of Si (by three orders of

746   magnitude) and O (about one order of magnitude) compared to rates measured in water-absent

747   mantle olivine (Dohmen et al., 2002b). Unlike the findings in dry conditions, diffusion rates

748   of Si and O are similar under water bearing conditions and diffusion anisotropy is weak to

749   absent. The high impact of H on Si diffusion can be understood by recognizing that the

750   concentration of Si vacancies is about 4 orders of magnitude smaller than the amount of H

751   that can be incorporated in olivine at the same conditions. Therefore, even a small fraction of

752   the total incorporated H is capable of substantially increasing the concentration of defects

753   responsible for diffusion of Si. The relation between the water fugacity and the Si diffusion

754   rates seems to obey a power law with a water fugacity exponent of 0.2 to 1; the latter

755   exponent is the same as that derived for dislocation creep of olivine. This indicates a strong

756   connection between Si diffusion and deformation. However, the activation energy for

757   dislocation creep is significantly higher (by ca. 100 - 150 kJmol^{-1}) than that for diffusion of

758   Si, whereas it is within error the same as that for O diffusion. This is consistent with the

759   observation that Si and O diffusion rates are similar under "wet" conditions, so that the two

760   processes control different aspects of dislocation creep. For all the transport properties

761   considered (volume diffusion and dislocation creep) the change in behavior from "dry" to

762   "water bearing" conditions occurs at low H concentration (e.g., < 10 ppm of H_2O in olivine at

763   2 GPa and 1200 ^{o}C). These values are lower than or overlap with those obtained from many

764   olivine crystals from mantle xenoliths. The implication is that even if the mantle is far from

765   water saturated, the influence of water on kinetic data needs to be considered for

766   understanding the physical and chemical behavior and evolution of the upper mantle - a

767   petrologically dry mantle may be rheologically and kinetically wet.

768

769   **10. Acknowledgements**

779

780   **11. References**

781   Bai, Q., Kohlstedt, D.L., 1992. Substantial hydrogen solubility in olivine and implications for

782   water storage in the mantle. Nature 357, 672-674.

783   Bai, Q., Kohlstedt, D.L., 1993. Effects of Chemical Environment on the Solubility and

784   Incorporation Mechanism for Hydrogen in Olivine. Phys. Chem. Min. 19, 460-471.

785   Béjina, F., Jaoul, O., Liebermann, R.C., 1999. Activation volume of Si diffusion in San

786   Carlos olivine: Implications for upper mantle rheology. J. Geophys. Res. 104, 25529-

787   25542.

788   Bell, D.R., Rossman, G.R., 1992. Water in Earths Mantle - the Role of Nominally Anhydrous

789   Minerals. Science 255, 1391-1397.

790   Bell, D.R., Rossman, G.R., Maldener, J., Endisch, D., Rauch, F., 2003. Hydroxide in olivine:

791   A quantitative determination of the absolute amount and calibration of the IR spectrum. J.

792   Geophys. Res. 108., doi: 1029/2001JB000679

793   Beran, A., Libowitzky, E., 2006. Water in natural mantle minerals II: Olivine, garnet and

794   accessory minerals. In: Keppler, H., Smyth, J.R., (Eds.), Water in nominally anhydrous

795   minerals. Reviews in Mineralogy and Geochemistry 62, 169-191.

796   Beran, A., Putnis, A., 1983. A Model of the Oh Positions in Olivine, Derived from Infrared-

797   Spectroscopic Investigations. Phys. Chem. Min. 9, 57-60.

798   Bercovici, D., Karato, S., 2003. Whole-mantle convection and the transition-zone water filter.

799   Nature 425, 39-44.

800   Berry, A.J,, Hermann, J., O'Neill, H.S.C., Foran, G.J., 2005. Fingerprinting the water site in

801   mantle olivine. Geology, 33, 869-872.

802   Billen, M.I., Gurnis, M., 2001. A low viscosity wedge in subduction zones. Earth Planet. Sci.

803   Lett. 193, 227-236.

804   Bolfan-Casanova, N., 2005. Water in the Earth's mantle. Min. Mag. 69, 229-257.

805   Bose, K., Ganguly, J., 1995a. Quartz-Coesite transition revisited - reversed experimental-

806   determination at 500-1200 ^{o}C and retrieved thermochemical properties. Am. Mineral. 80,

807   231-238.

808   Bose, K., Ganguly, J., 1995b. Experimental and theoretical studies of the stabilities of talc,

809   antigorite and phase A at high pressures with applications to subduction processes. Earth

810   Planet. Sci. Lett. 136, 109 - 121.

811   Braithwaite, J.S., Wright, K., Catlow, C.R.A., 2003. A theoretical study of the energetics and

812   IR frequencies of hydroxyl defects in forsterite. J. Geophys. Res. 108.

813   doi:10.1029/2002JB002126

814   Brodholt, J.P., Refson, K., 2000. An ab initio study of hydrogen in forsterite and a possible

815   mechanism for hydrolytic weakening. J. Geophys. Res. 105, 18977-18982.

816   Chakraborty, S., Ganguly, J., 1992. Cation diffusion in aluminosilicate garnets -

817   experimental-determination in spessartine-almandine diffusion couples, evaluation of

818   effective binary diffusion-coefficients, and applications. Contrib. Mineral. Petrol. 111, 74-

819   86.

820   Chakraborty, S., Rubie, D.C., 1996. Mg tracer diffusion in aluminosilicate garnets at 750-850

821   ^{o} C, 1 atm and 1300° C, 8.5 GPa. Contrib. Mineral. Petrol. 122, 406-414.

822   Connolly, J.A.D., 1990. Multivariable phase-diagrams - an algorithm based on generalized

823   thermodynamics. Am. J. Sci. 290, 666-718.

824   Demouchy, S., Mackwell, S., 2003. Water diffusion in synthetic iron-free forsterite. Phys.

825   Chem. Min. 30, 486-494.

826   Demouchy, S., Mackwell, S., 2006. Mechanisms of hydrogen incorporation and diffusion in

827   iron-bearing olivine. Phys. Chem. Min. 33, 347-355.

828   Demouchy, S., Mackwell, S., Kohlstedt, D., 2007. Influence of hydrogen on Fe–Mg

829   interdiffusion in (Mg,Fe)O and implications for Earth's lower mantle. Contrib. Mineral.

830   Petrol. in press

831   Dimos, D., Wolfenstine, and Kohlstedt, D.L., 1988. Kinetic demixing and decomposition of

832   multicomponent oxides due to a nonhydrostatic stress. Acta Metall. 36, 1543-1552.

833 Dixon, J.E., Dixon, T.H., Bell, D.R., Malservisi, R., 2004. Lateral variation in upper mantle

834   viscosity: role of water. Earth Planet. Sci. Lett. 222, 451-467.

835 Dohmen, R., Chakraboty, S., 2007. Fe-Mg diffusion in olivine II: point defect chemistry,

836   change of diffusion mechanism and a model for calculation of diffusion coefficients in

837   natural olivine. Phys. Chem. Min., in press

838 Dohmen, R., Chakraborty, S., Becker, H.W., 2002b. Si and O diffusion in olivine and

839   implications for characterizing plastic flow in the mantle. Geophys. Res. Lett. 29.

840   doi:10.1029/2002GL015480.

841 Dohmen, R., Becker H.-W., Chakraborty, S., 2007. Fe-Mg diffusion in olivine I: Experiments

842   determination between 700 and 1200 ^{o}C as a function of composition, crystal orientation

843   and oxygen fugacity. Phys. Chem. Min., in press.

844 Dohmen, R., Becker, H.W., Meissner, E., Etzel, T., Chakraborty, S., 2002a. Production of

845   silicate thin films using pulsed laser deposition (PLD) and applications to studies in

846   mineral kinetics. Eur. J. Min. 14, 1155-1168.

847 Elphick, S.C., Ganguly, J., Loomis, T.P., 1985. Experimental-determination of cation

848   diffusivities in aluminosilicate garnets .1. experimental methods and interdiffusion data.

849   Contrib. Mineral. Petrol. 90, 36-44.

850 Evans, H.E., Knowles, G., 1978. Dislocation Creep in Non-Metallic Materials. Acta Metall.

851   26, 141-145.

852 Farber, D.L., Williams, Q., Ryerson, F.J., 2000. Divalent cation diffusion in Mg2SiO4 spinel

853   (ringwoodite), beta phase (wadsleyite), and olivine: Implications for the electrical

854   conductivity of the mantle. J. Geophys. Res. 105, 513-529.

855 Freed, A.M., Bürgmann, R., 2004. Evidence of power-law flow in the Mojave desert mantle.

856   Nature 430, 548-551.

857   Ganguly, J., Bhattacharya, R.N., Chakraborty, S., 1988. Convolution effect in the

858   determination of compositional profiles and diffusion-coefficients by microprobe step

859   scans. Am. Mineral. 73, 901-909.

860   Ganguly, J., Cheng, W.J., Chakraborty, S., 1998. Cation diffusion in aluminosilicate garnets:

861   experimental determination in pyrope-almandine diffusion couples. Contrib. Mineral.

862   Petrol. 131, 171-180.

863   Gérard, O., Jaoul, O., 1989. Oxygen Diffusion in San-Carlos Olivine. J. Geophys. Res. 94,

864   4119-4128.

865   Ghiorso, M.S., Carmichael, I.S.E., 1987. Modeling magmatic systems - petrologic

866   applications. In: Carmichael, I.S.E., Eugster, H.P., (Eds.), Thermodynamic modelling of

867   geological materials: minerals, fluids and melts. Reviews in Mineralogy 17, 467-499.

868   Goldsmith, J.R., 1991. Pressure enhanced Al/Si diffusion and oxygen isotope exchange, In:

869   Ganguly, J. (Ed.), Diffusion, atomic ordering, and mass transport, Advances in Physical

870   Chemistry, 8, pp. 221-247.

871   Graham, C.M., Elphick, S.C., 1991. Some experimental constraints on the role of hydrogen in

872   oxygen and hydrogen diffusion an Al-Si interdiffusion in silicates, In: Ganguly, J. (Ed.),

873   Diffusion, atomic ordering, and mass transport, Advances in Physical Chemistry, 8, pp.

874   248-303.

875   Hauri, E.H., Gaetani, G.A., Green, T.H., 2006. Partitioning of water during melting of the

876   Earth's upper mantle at H2O-undersaturated conditions. Earth Planet. Sci. Lett. 248, 715-

877   734.

878   Hier-Majumder, S., Anderson, I.M., Kohlstedt, D.L., 2005. Influence of protons on Fe-Mg

879   interdiffusion in olivine. J. Geophys. Res. 110, doi:10.1029/2004JB003292.

880   Hirschmann, M.M., 2006. Water, melting, and the deep Earth H_2O cycle. Ann. Rev. Earth

881   Planet. Sci. 34, 629-653.

882   Hirth, G., Kohlstedt, D.L., 1996. Water in the oceanic upper mantle: Implications for

883   rheology, melt extraction and the evolution of the lithosphere. Earth Planet. Sci. Lett. 144,

884   93-108.

885   Hirth, G., Kohlstedt, D., 2003. Rheology of the upper mantle and the mantle wedge: a view

886   from the experimentalist. In: Eiler, J., (Ed), Inside the subduction factory, American

887   Geophysical Union, Monograph 138, 83-105.

888   Hobbs, B.E., 1984. Point-defect chemistry of minerals under a hydrothermal environment. J.

889   Geophys. Res. 89, 4026-4038.

890   Holland, T.J.B., Powell, R., 1998. An internally consistent thermodynamic data set for phases

891   of petrological interest. J. Metam. Geol. 16, 309-343.

892   Holloway, J.R., 1981. Compositions and volumes of supercritical fluids in the Earth's crust.

893   In: Hollister, L.S., Crawford, M.L. (Eds.), Fluid inclusions, applications to petrology,

894   Mineralogical Association of Canada, 13-38.

895   Holloway, J.R., 1987. Igneous fluids. In: Carmichael, I.S.E., Eugster, H.P. (Eds.)

896   Thermodynamic modelling of geological materials: minerals, fluids and melts. Reviews in

897   Mineralogy 17, 211-233.

898   Holzapfel, C., Chakraborty, S., Rubie, D.C., Frost, D.J., 2007. Effect of pressure on Fe-Mg,

899   Ni and Mn diffusion in (FexMg1-x)SiO4. Phys. Earth Planet. Int. in press.

900   Houlier, B., Cheraghmakani, M., Jaoul, O., 1990. Silicon Diffusion in San-Carlos Olivine.

901   Phys. Earth Planet. Int. 62, 329-340.

902   Huebner, J.S., Sato, M., 1970. Oxygen Fugacity-Temperature Relationships of Manganese

903   Oxide and Nickel Oxide Buffers. Am. Mineral. 55, 934-952.

904   Ingrin. J., Skogby, H., 2000. Hydrogen in nominally anhydrous upper-mantle minerals:

905   concentration levels and implications. Eur. J. Mineral 12, 543-570.

906 Jaoul, O., 1990. Multicomponent Diffusion and Creep in Olivine. J. Geophys. Res. 95, 17631-

907   17642.

908 Johnson, M.C., Walker, D., 1993. Brucite [Mg(OH)$_2$] dehydration and the molar volume of

909   H$_2$O to 15 GPa. Am. Mineral. 78, 271-284.

910 Karato, S., 2006. Influence of hydrogen-related defects on the electrical conductivity and

911   plastic deformation of mantle minerals: A critical review, In: Jacobsen, S.D., van der Lee,

912   S., (Eds.), Earth's deep water cycle, Gephysical Monograph Series 168, 113-130.

913 Karato, S.I., Jung, H., 2003. Effects of pressure on high-temperature dislocation creep in

914   olivine. Phil. Mag. 83, 401-414.

915 Keppler, H., Bolfan-Casanova, N., 2006. Thermodynamics of water solubility and

916   partitioning, In: Keppler, H., Smyth, J.R., (Eds.), Water in nominally anhydrous minerals.

917   Reviews in Mineralogy and Geochemistry 62, 193-230.

918 Koch-Müller, M., Matsyuk, S.S., Rhede, D., Wirth, R., Khisina, N., 2006. Hydroxyl in mantle

919   olivine xenocrysts from the Udachnaya kimberlite pipe. Phys. Chem. Min. 33, 276-287.

920 Kohlstedt, D.L., 2006. The role of water in high-temperature rock deformation, In: Keppler,

921   H., Smyth, J.R., (Eds.), Water in nominally anhydrous minerals. Reviews in Mineralogy

922   and Geochemistry 62, 377-396.

923 Kohlstedt, D.L., Mackwell, S.J., 1998. Diffusion of hydrogen and intrinsic point defects in

924   olivine. Z. Phys. Chem. 207, 147-162.

925 Kohlstedt, D.L., Mackwell, S.J., 1999. Solubility and diffusion of "water" in silicate minerals.

926   In: Wright, K., Catlow, R. (Eds.), Microscopic properties and processes in minerals,

927   Kluwer Academic Publishers, 539-559.

928 Kohlstedt, D.L., Keppler, H., Rubie, D.C., 1996. Solubility of water in the alpha, beta and

929   gamma phases of (Mg,Fe)(2)SiO4. Contrib. Mineral. Petrol. 123, 345-357.

39

930   Kohn, S.C., 2006. Structural studies of OH in nominally anhydrous minerals using NMR, In:

931   Keppler, H., Smyth, J.R., (Eds.), Water in nominally anhydrous minerals. Reviews in

932   Mineralogy and Geochemistry 62, 53-66.

933   Kröger, F.A., Vink, H.J., 1965. Relation between the concentrations of imperfections in

934   crystalline solids. In: Steiz, F., Turnball, D. (Eds.), Solid State Physics 3, 307-435.

935   Kurosawa, M., Yurimoto, H., Sueno, S., 1997. Patterns in the hydrogen and trace element

936   compositions of mantle olivines. Phys. Chem. Min. 24, 385-395.

937   Lemaire, C., Kohn, S.C., Brooker, R.A., 2004. The effect of silica activity on the

938   incorporation mechanisms of water in synthetic forsterite: a polarised infrared

939   spectroscopic study. Contrib. Mineral. Petrol. 147, 48-57.

940   Libowitzky, E., Rossman, G.R., 1996. Principles of quantitative absorbance measurements in

941   anisotropic crystals. Phys. Chem. Min. 23, 319-327.

942   Lithgow-Bertelloni, C., Richards, M.A., 1995. Cenozoic Plate Driving Forces. Geophys. Res.

943   Lett. 22, 1317-1320.

944   Mackwell, S.J., Kohlstedt, D.L., Paterson, M.S., 1985. The role of water in the deformation of

945   olivine single crystals. J. Geophys. Res. 90, 11319-11333

946   Mackwell, S.J., Dimos, D., Kohlstedt, D.L., 1988. Transient creep of olivine - point defect

947   relaxation times. Phil. Mag. 57, 779-789.

948   Mackwell, S.J., Kohlstedt, D.L., 1990. Diffusion of Hydrogen in Olivine - Implications for

949   Water in the Mantle. J. Geophys. Res. 95, 5079-5088.

950   Mao, H.K., Bell, P.M., England, J.L., 1971. Tensional errors and drift of the thermocouple

951   electromotive force in the single-stage piston-cylinder apparatus. Carnegie Inst. Wash.

952   Year Book 70, 281-287.

953   Matveev, S., O'Neill, H.S., Ballhaus, C., Taylor, W.R., Green, D.H., 2001. Effect of silica

954   activity on OH-IR spectra of olivine: Implications for low-aSiO(2) mantle metasomatism.

955   J. Pet. 42, 721-729.

956   Mei, S., Kohlstedt, D.L., 2000. Influence of water on plastic deformation of olivine

957   aggregates 2. Dislocation creep regime. J. Geophys. Res. 105, 21471-21481.

958   Miller, G.H., Rossman, G.R., Harlow, G.E., 1987. The natural occurrence of hydroxide in

959   olivine. Phys. Chem. Min. 14, 461-472.

960   Misener, D.J., 1974. Cationic diffusion in olivine to 1400 oC and 35 kbar. In: Hofmann,

961   A.W., Giletti, B.J., Yoder Jr, H.S., Yund, R.A., (Eds.), Geochemical and Transport

962   Kinetics, Carnegie Institution of Washington, 117-138.

963   Mosenfelder, J.L., Deligne, N.I., Asimow, P.D., Rossman, G.R., 2006. Hydrogen

964   incorporation in olivine from 2-12 GPa. Am. Mineral. 91, 285-294.

965   Nabarro, F.R.N., 1967. Steady-State Diffusional Creep. Phil. Mag. 16, 231-237.

966   Nakamura, A., Schmalzried, H., 1983. On the nonstoichiometry and point-defects of olivine.

967   Phys. Chem. Min. 10, 27-37.

968   Nix, W.D., Gascaner.R, Hirth, J.P., 1971. Contribution to Theory of Dislocation Climb. Phil.

969   Mag. 23, 1339-1349.

970   Paterson, M.S., 1982. The determination of hydroxyl by infrared-absorption in Quartz,

971   silicate-glasses and similar materials. Bull. Mineral. 105, 20-29.

972   Pawley, A.R., and Wood, B.J., 1995. The high-pressure stability of talc and 10 Å phase:

973   potential storage sites for H_2O in subduction zones. Am. Mineral. 80, 998-1003.

974   Pichavant, M., Mysen, B.O., Macdonald, R., 2002. Source and H2O content of high-MgO

975   magmas in island arc settings: An experimental study of a primitive calc-alkaline basalt

976   from St. Vincent, Lesser Antilles arc. Geochim. Cosmochim. Acta 66, 2193-2209.

977   Pitzer, K.S., Sterner, S.M., 1994. Equations of state valid continuously from zero to extreme

978   pressures for H_2O and CO_2. J. Chem. Phys. 101, 3111-3116.

979   Regenauer-Lieb, K., 2006. Water and geodynamics, In: Keppler, H., Smyth, J.R., (Eds.),

980   Water in nominally anhydrous minerals. Reviews in Mineralogy and Geochemistry 62,

981   451-474.

982   Robie, R.A., Hemingway, B.S., 1995. Thermodynamic properties of minerals and related

983   substances at 298.15 K and 1 bar (10^5 Pascals) pressure and at higher temperatures. U.S.

984   Geol. Surv. Bull. 2131, 461 pp.

985   Ruoff, A.L., 1965. Mass transfer problems in ionic crystals with charge neutrality. J. App.

986   Phys. 36, 2903-2907.

987   Ryerson, F.J., Durham, W.B., Cherniak, D.J., Lanford, W.A., 1989. Oxygen diffusion in

988   olivine - effect of oxygen fugacity and implications for creep. J. Geophys. Res. 94, 4105-

989   4118.

990   Schmalzried, H., 1974. Solid State reactions. Weinheim, Verlag Chemie, 214 pp.

991   Smyth, D.M., Stocker, R.L., 1975. Point defects and non-stoichiometry in forsterite. Phys.

992   Earth Planet. Int. 10, 183-192.

993   Stocker, R.L., Smyth, D.M., 1978. Effect of enstatite activity and oxygen partial pressure on

994   the point-defect chemistry of olivine. Phys. Earth Planet. Int. 16, 145-156.

995   Tingle, T.N., 1988. Retrieval of uncracked single-crystals from high-pressure in piston-

996   cylinder apparatus. Am. Mineral. 73, 1195-1197.

997   Tsai, T.L., Dieckmann, R., 2002. Variation of the oxygen content and point defects in

998   olivines, (Fex Mg1-x)2SiO4, 0.2 = x = 1.0. Phys. Chem. Min. 29, 680-694.

999   Walker, A.M., Wright, K., Slater, B., 2003. A computational study of oxygen diffusion in

1000   olivine. Phys. Chem. Min. 30, 536-545.

1001   Wanamaker, B.J., 1994. Point-Defect Diffusivities in San Carlos Olivine Derived from

1002   Reequilibration of Electrical-Conductivity Following Changes in Oxygen Fugacity.

1003   Geophys. Res. Lett. 21, 21-24.

1004   Wang, D.J., Mookherjee, M., Xu, Y.S., Karato, S., 2006. The effect of water on the electrical

1005   conductivity of olivine. Nature 443, 977-980.

1006   Wang, Z.Y., Hiraga, T., Kohlstedt, D.L., 2004. Effect of H+ on Fe-Mg interdiffusion in

1007   olivine, (Fe,Mg)(2)SiO4. Appl. Phys. Lett. 85, 209-211.

1008   Watson, E.B., Wark, D.A., Price, J.D., Van Orman, J.A. 2002. Mapping the thermal structure

1009   of solid-media pressure assemblies. Contrib. Mineral. Petrol. 142, 640-652.

1010   Weertman, J., 1999. Microstructural mechanisms of creep. In: Meyers, M.A., Armstrong,

1011   R.W., Kirschner, H. (Eds.) Mechanics and Materials: Fundamentals and Linkages, John

1012   Wiley & Sons, 451-488.

1013   Wright, K., 2006. Atomistic models of OH defects in nominally anhydrous minerals, In:

1014   Keppler, H., Smyth, J.R., (Eds.), Water in nominally anhydrous minerals. Reviews in

1015   Mineralogy and Geochemistry 62, 67-83.

1016   Yoshino, T., Matsuzaki, T., Yamashita, S., Katsura, T., 2006. Hydrous olivine unable to

1017   account for conductivity anomaly at the top of the asthenosphere. Nature 443, 973-976.

1018   Zhao, Y.H., Ginsberg, S.B., Kohstedt, D.L., 2004. Solubility of hydrogen in olivine:

1019   dependence on temperature and iron content. Contrib. Mineral. Petrol. 147, 155-161.

1020

1021

Figure captions

1023

1024 **Figure 1**: (a) olivine crystal plus thin films of olivine enriched in ^{18}O and ^{29}Si plus a

1025 protective thin film of ZrO_2. (b) A sandwich of two olivine crystals was used in the

1026 experiments. This setting prevented olivine thin films from reacting with the environment and

1027 yielded two crystals per anneal, providing a check for reproducibility of data.

1028

1029 **Figure 2**: (a) Breakdown of olivine to orthopyroxene and magnesite or melting of olivine in

1030 the presence of high water content limit the ranges of P-T over which experiments can be

1031 carried out. Solid lines are for pure forsterite, and dotted lines are estimated positions for Fo_{90}.

1032 The pressure-temperature conditions of two experiments are marked as circles and textures

1033 observed on the respective run products are shown in the (b) and (c) parts of the figure. (b)

1034 SEM image of olivine surface after high-P and T annealing [precise conditions shown in (a)].

1035 One can see a reaction texture where olivine is transformed to orthopyroxene (light grey) and

1036 magnesite (dark grey). (c) Surface of the olivine after annealing within its stability filed

1037 [lower P and T, see circle in (a)]. The thin film looks like a fine-grained recrystallized

1038 material appropriate for determining diffusion data (e.g., Dohmen et al., 2002a; Dohmen et

1039 al., 2007).

1040

1041 **Figure 3**: Sketch of cell assembly used in the piston-cylinder experiments.

1042

1043 **Figure 4.** Photomicrographs of olivine crystal annealed at 2 GPa, 1225 ^{o}C and with water

1044 present. This crystal was quickly (*ca.* 1 minute) quenched from run to near ambient

1045 conditions. It shows polyphase crystallographically-oriented inclusions made of opaque

44

1046   phases and bubbles, Sample 40F2TR. These inclusions are not present in the slowly quenched

1047   runs.

1048

1049   **Figure 5.** A typical experiment took about 30 minutes to go from the high P and T conditions

1050   to near room P, T and the paths (80-90°C and 0.07 GPa per minute, respectively) are shown in

1051   (a). We have modeled the effect of such a P-T-t path on the water content of the olivine by

1052   incorporating the T dependence of the diffusion coefficient of H from Kohlstedt and

1053   Mackwell (1998) in a diffusion model with a changing boundary condition according to the T

1054   and P dependence of the water fugacity using the equation of state of Pitzer and Sterner

1055   (1994) and the solubility model of Zhao et al. (2004). Thus the water content at the boundary

1056   is the maximum allowed solubility at a given P and T in the presence of a pure water fluid. (b)

1057   Model calculations of diffusive reequilibration in one dimension for a 1.5 mm thick slab using

1058   the diffusion data parallel to *a* axis. Numbers on the left of the calculated profiles are the

1059   times in minutes and numbers on the right are the amount of water (averaged through the

1060   crystal expressed in % with respect to the starting value) that remains. It is apparent that with

1061   the P-T-t paths we used in our experiments and which were required to retrieve crystals in

1062   good physical condition to be analyzed for diffusion, crystals can loose up to 50 % of their

1063   water content. Such a change is consistent with the difference in total water contents analyzed

1064   by FTIR from quickly and slowly quenched runs (Table 1).

1065

1066   **Figure 6.** FTIR spectra of three olivines annealed at different P, T, $f\text{H}_2\text{O}$ and $f\text{O}_2$ conditions.

1067   Black spectra are parallel to the *a* axis and gray spectra parallel to the *b* axis. The size of the

1068   peaks at 3612 and 3600 cm^{-1} decrease with total water content to the extent that in the samples

1069   with the very low water (8 ppm) they are absent, a new peak appears at ca 3527 cm^{-1}, and the

1070   peak at ca 3579 cm^{-1} decreases and shifts to 3571 cm^{-1}. The asterisk next to the $f\text{H}_2\text{O}$ and $f\text{O}_2$

1071   values of the slowly cooled run is to highlight that these were calculated at the experimental

1072   conditions and are not related to the measured low water contents affected by the slow cooling

1073   and decompression path and loss of H (e.g., Fig.5 and text for discussion).

1074

1075   **Figure 7**: Example of fits of diffusion models to the isotope concentration profiles. The initial

1076   concentration distributions were obtained in unannealed crystals. The ZrO_2 layer is not

1077   detected because its O and Si isotopes have probably been homogenized by exchange with the

1078   olivine thin film. Note that the O diffusion profile (a) shows that the olivine thin film has also

1079   exchanged isotopes with the surrounding fluid.

1080

1081   **Figure 8**: Arrhenius plot for diffusion data of Si. The dashed lines are the 95 % confidence

1082   intervals of the predicted values. Cross on upper left corner shows the magnitude of the error

1083   of D_{Si} and T.

1084

1085   **Figure 9**: Arrhenius plot for diffusion data of O. The dashed lines are the 95 % confidence

1086   intervals of the predicted values. Cross on upper left corner shows the magnitude of the error

1087   of D_O and T.

1088

1089   **Figure 10**: Comparison of dry and water-bearing diffusion data of O and Si from various

1090   sources. [R89] = Ryerson et al. (1989), [G&J89] = Gérard and Jaoul (1989), [D02]= Dohmen

1091   et al. (2002b).

1092

1093   **Figure 11**. Schematic diagram showing how the water fugacity exponents (r values) and the

1094   wet to dry transition (fH_2O^* values) can be determined graphically. See text for more

1095   explanation.

1096

1097   **Figure 12.** Water fugacity exponents and dry to wet transitions for Si and O at 1200 $^{\circ}$C and 2

1098   GPa. (a) The available data for Si at two fH$_2$O can be reproduced by water exponents between

1099   1 and 0.2. The diffusion coefficient at dry conditions (e.g., horizontal line) is that of Dohmen

1100   et al. (2002b) using an activation volume of 7 m^{3}mol^{-1} as discussed in the text. (b) Because

1101   we have been able to retrieve the diffusion coefficient of O at a single fH$_2$O we can not put

1102   strong constraint on the precise value of the fH$_2$O exponent for this element. Abbreviations for

1103   the references of the water absent data are as in Fig. 10.

1104

1105   **Figure 13.** Water fugacity exponents and dry to wet transitions for different transport

1106   properties in forsterite-rich single crystal olivine or aggregates. (a) Fe-Mg diffusion. Dry

1107   diffusion parameters from Dohmen and Chakraborty (2007) and Holzapfel et al. (2007).

1108   Water-bearing parameters from Hier-Majumder et al. (2005). (b) Dislocation creep

1109   parameters from the review of Hirth and Kohlstedt (2003).

1110

1111   **Figure 14.** Strain rates calculated using three different dislocation creep models that involve

1112   the role of climb as rate limiting step. [W99] is the model of Weertman (1999), [N68] refers

1113   to the model of Nabarro (1968) and [E&K78] refers to that of Evans and Knowles (1978). The

1114   flow law was calculated using the constant fugacity values and parameters found in Hirth and

1115   Kohlstedt (2003). The numbers next to the Weertman models are different values of λ_g/λ_c.

1116   The diffusion coefficient that was used in the dislocation creep models is 2.7 10^{-20} m^{2}s^{-1} and

1117   corresponds to D$_{Si}$ at 1200 $^{\circ}$C, 2GPa and fH$_2$O = 0.97 GPa (Table 1). Other values used are as

1118   in Kohlstedt (2006) with G = 52 GPa, b = 0.485 nm, V$_m$ = 43.8 $\cdot 10^{-6}$ m^3, ν = 0.245. Note

1119   good agreement between the flow law and the Evans and Knowles (1977) at low differential

1120   stress and with that of Weertman (1999) for λ_g/λ_c values between 1 and 10 indicating that the

1121   role of climb is important in determining the dislocation creep rates.

1122   **Table 1.** Experimental conditions and diffusion coefficients in San Carlos olivine

1123

1124   **Table 2.** Do ,E and deltaV for diffusion and deformation and recalculated values

1125

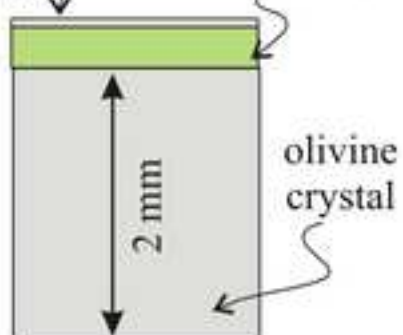1126   **Table 3.** Dry to wet transition water fugacity (f_{H2O}^*)and concentrations

1127

1128   **Table 4.** Point defect concentration calculations

(a)

ZrO$_2$
thin film
< 100 nm

Thin film (~ 500 nm), same
composition as the crystal but
enriched in ^{29}Si, ^{18}O

(b) setting used for experiments:
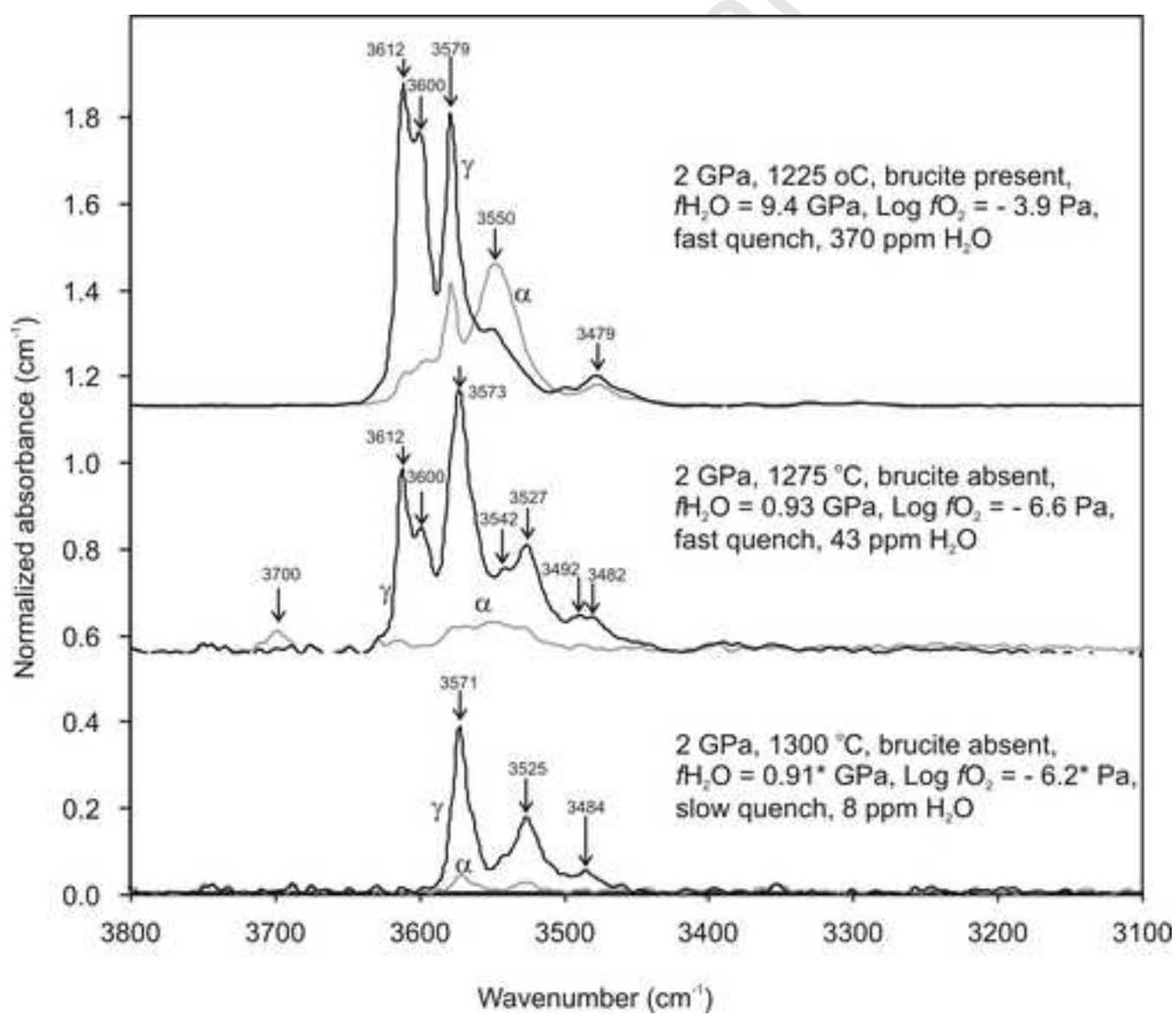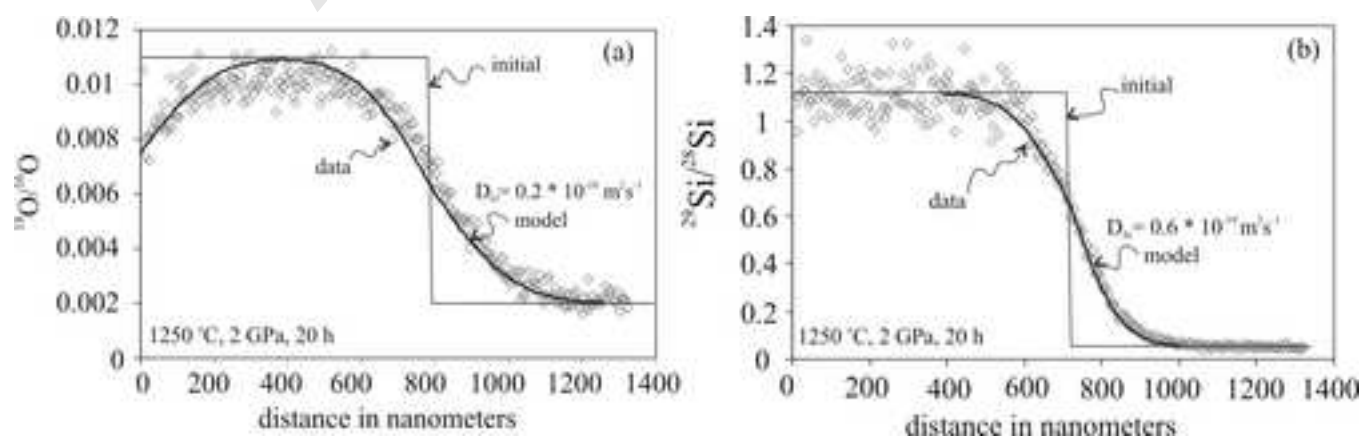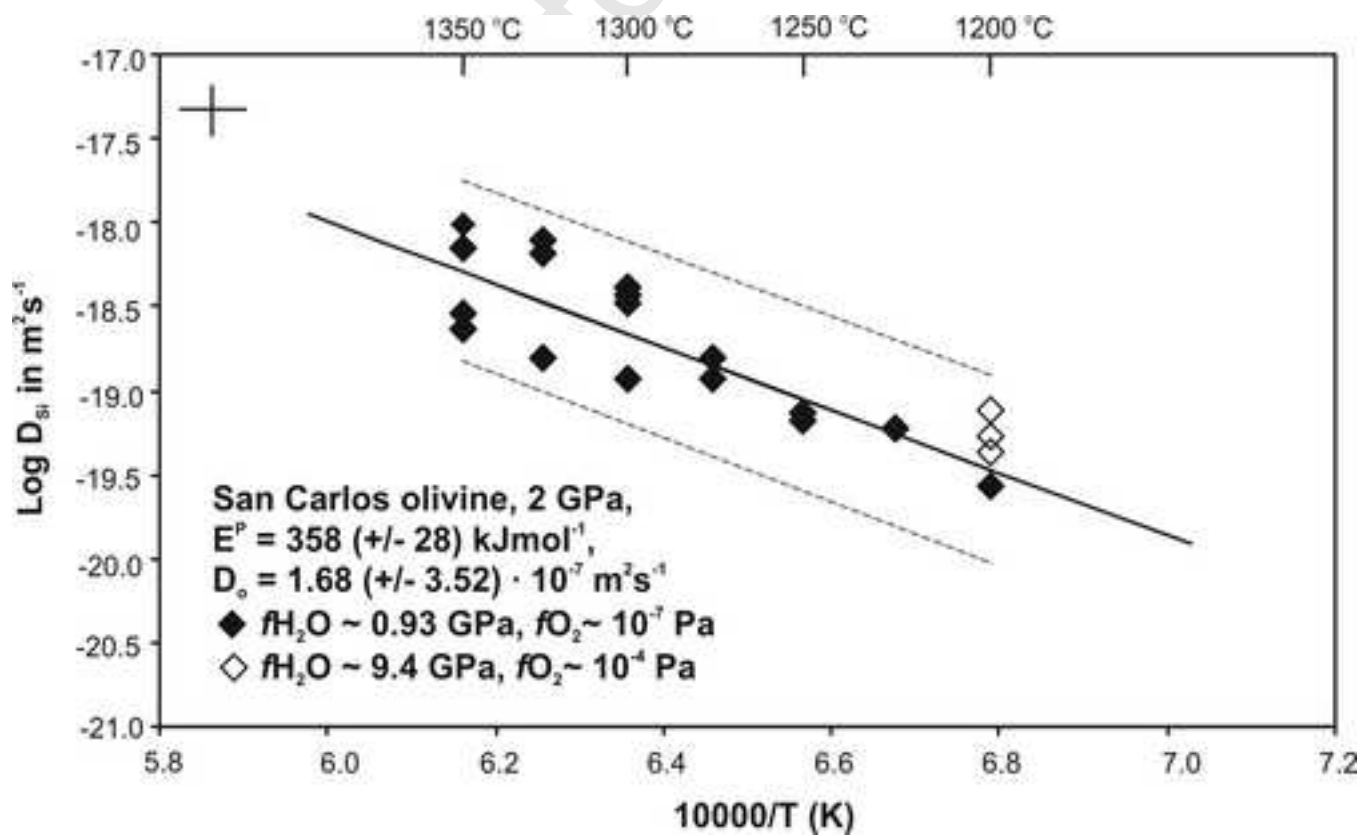two olivine crystals
plus thin films
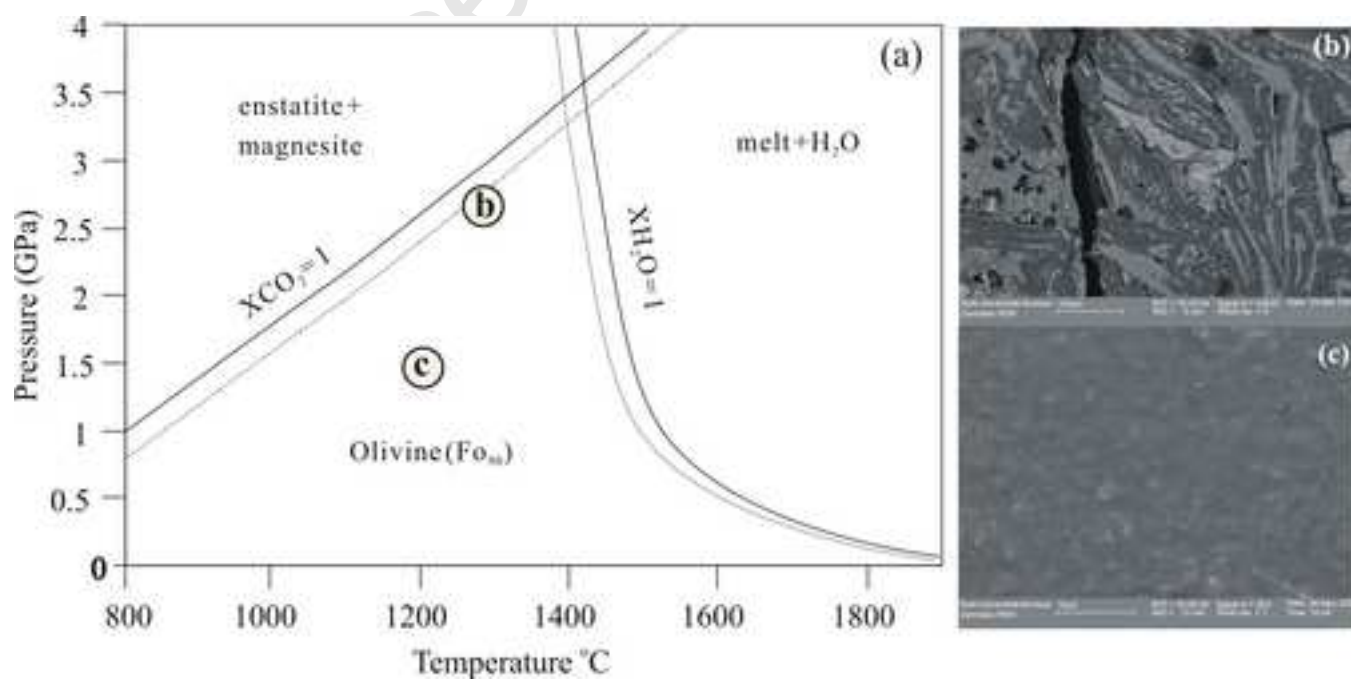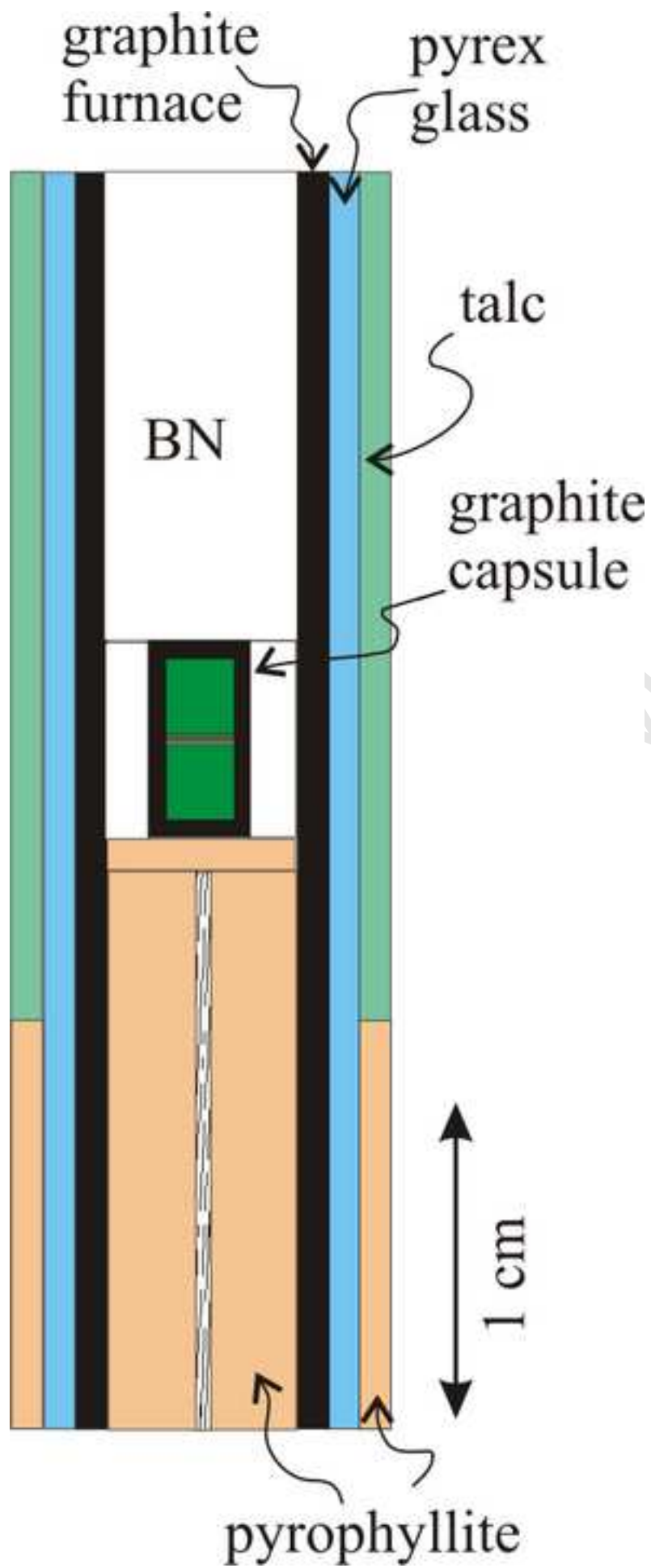
2 mm

olivine
crystal

Si, [this work],
2 GPa, fH_2O = 0.93 GPa
360 kJmol^{-1}

fO_2 =10^{-4} Pa
330 kJmol^{-1}

O, [this work],
2 GPa,
fH_2O = 0.93 GPa

O, [R89],
320 kJmol^{-1}
fO_2 =10^{-4} Pa

buffer fO_2,
437 kJmol^{-1}

O, [D02]
340 kJmol^{-1}
fO_2 =10^{-4} Pa

O, [G&J89]
266 kJmol^{-1}
fO_2 =10^{-4} Pa

Si, [D02],
530 kJmol^{-1}

Olivine (*ca*. Fo$_{90}$)

Log D in m^{2}s^{-1}

10000/ TK
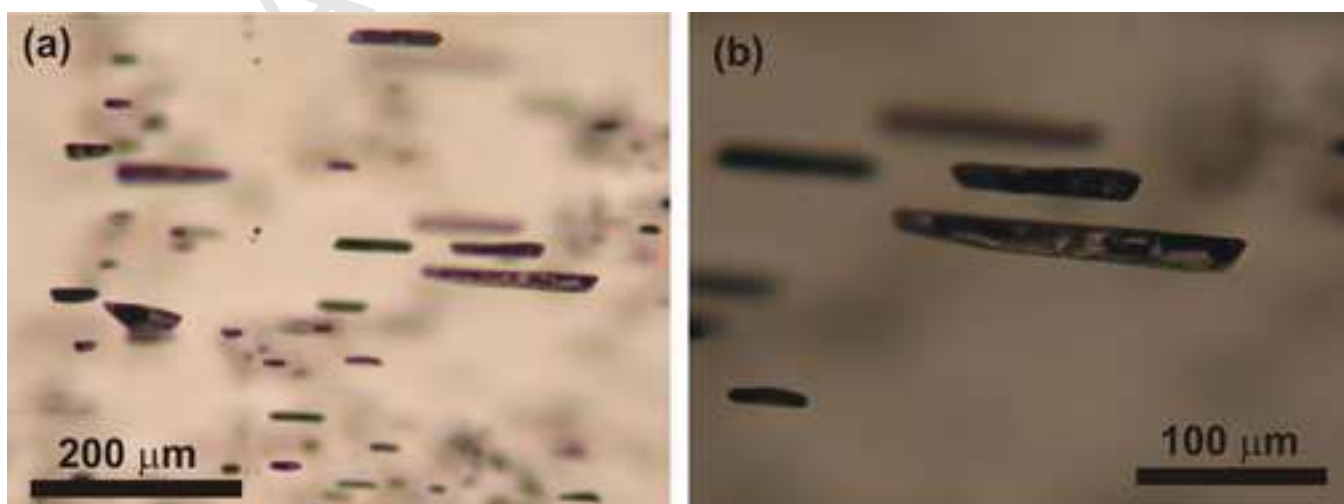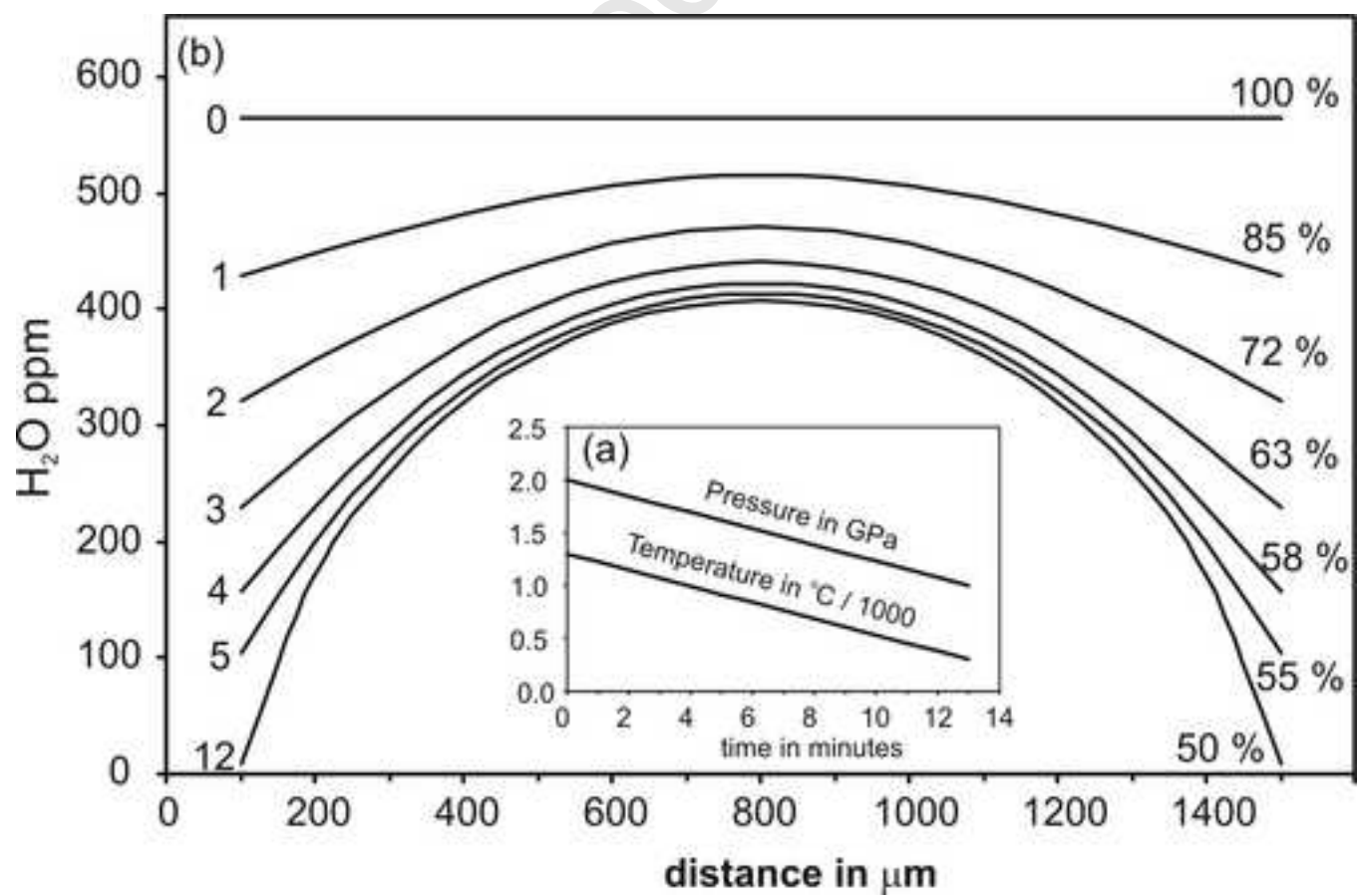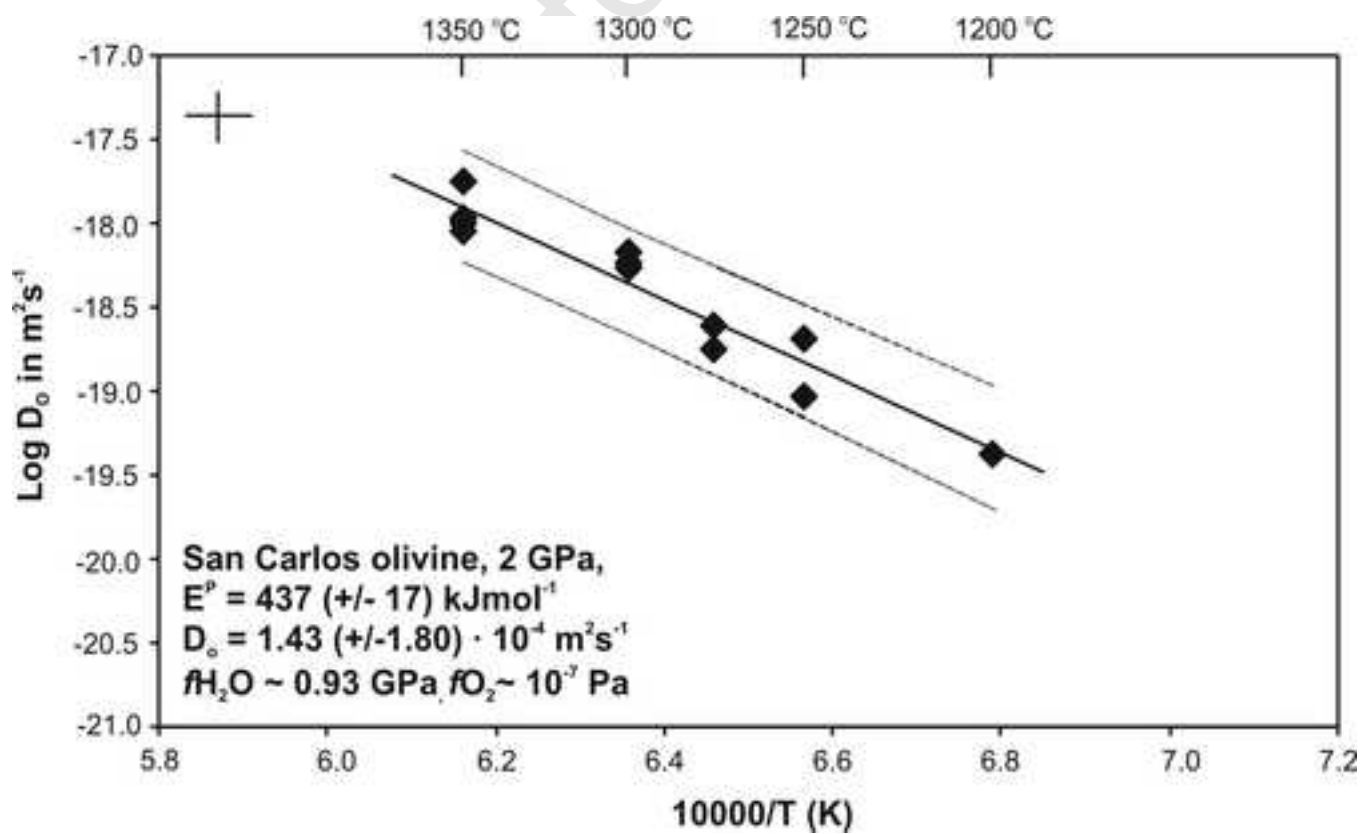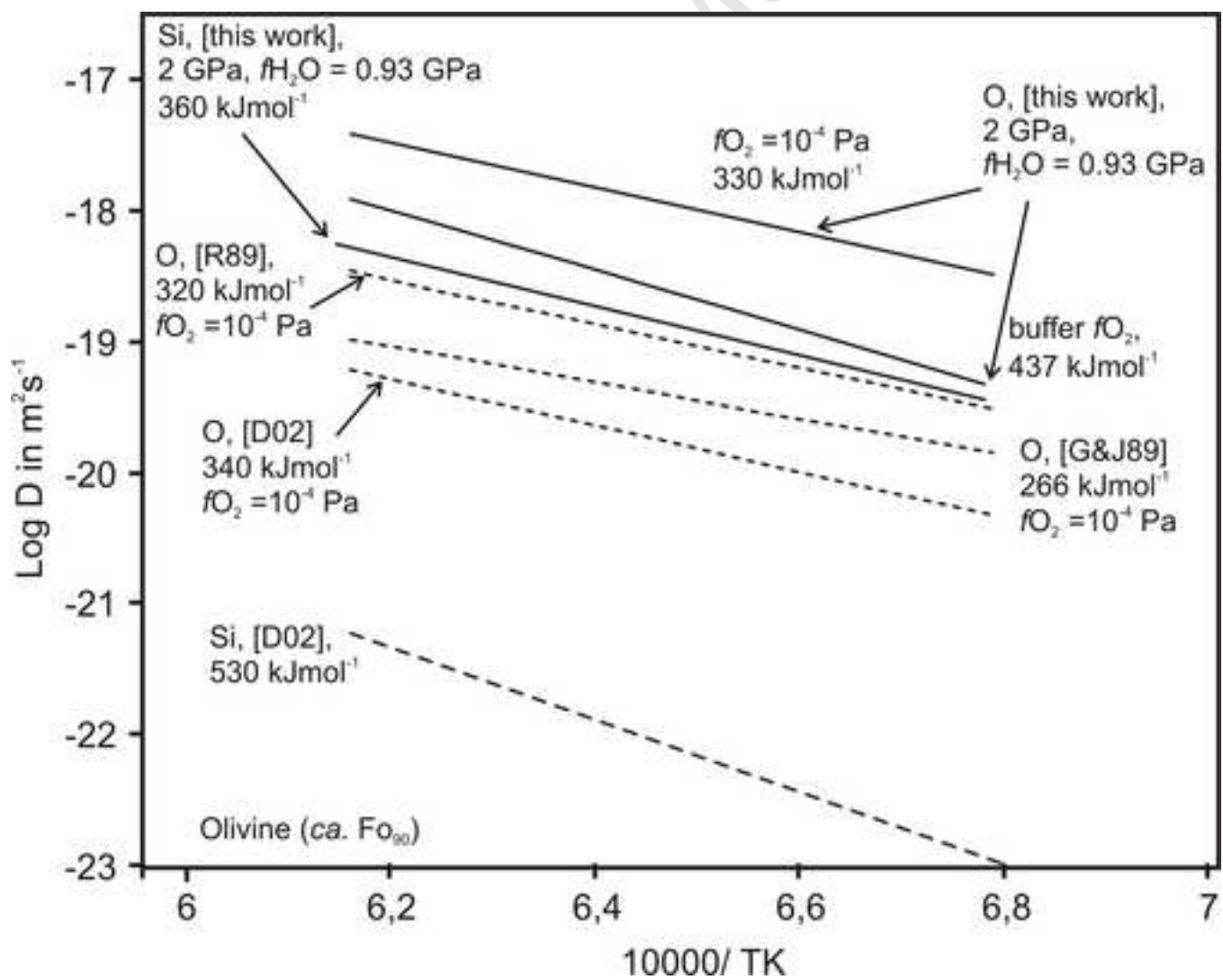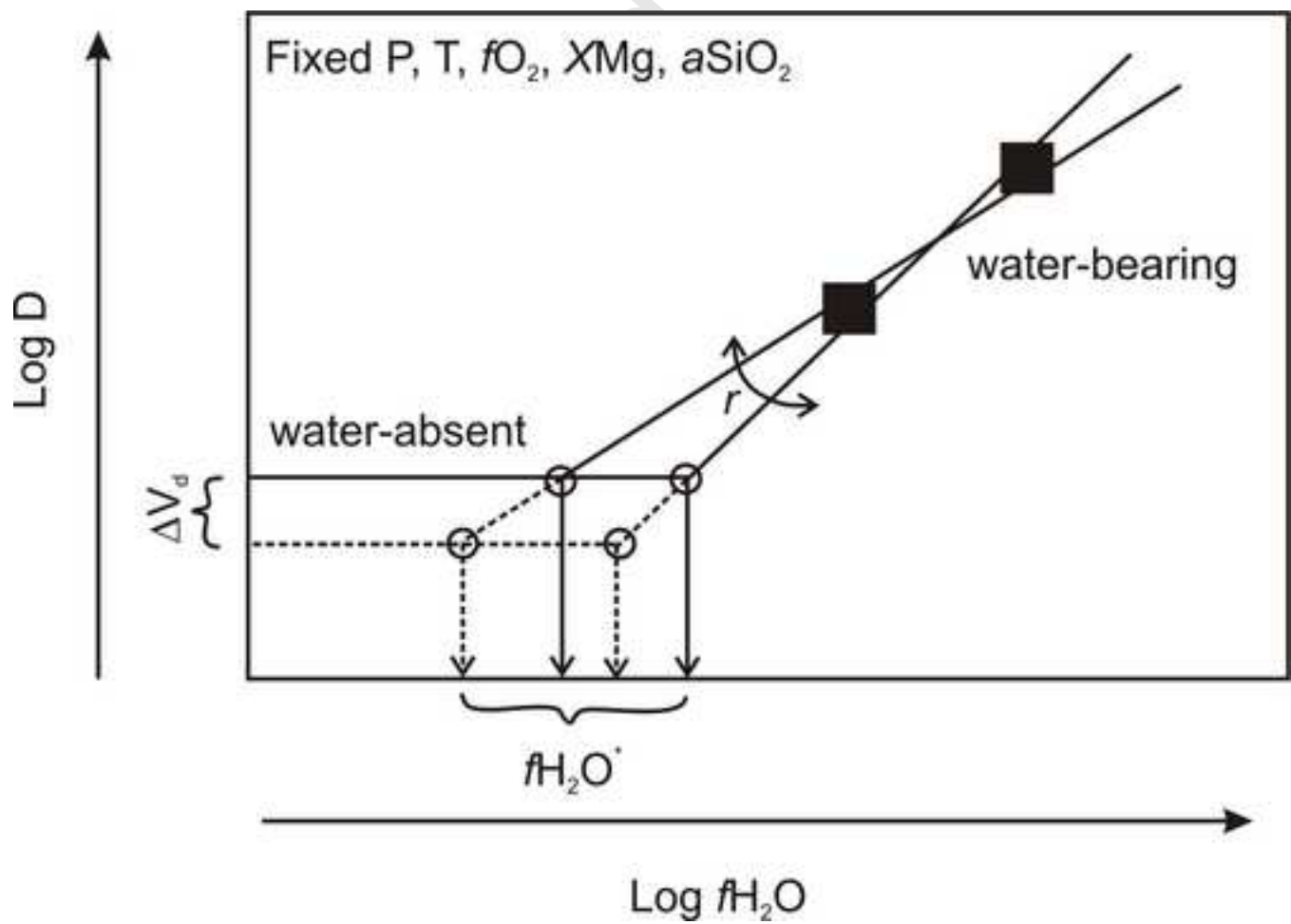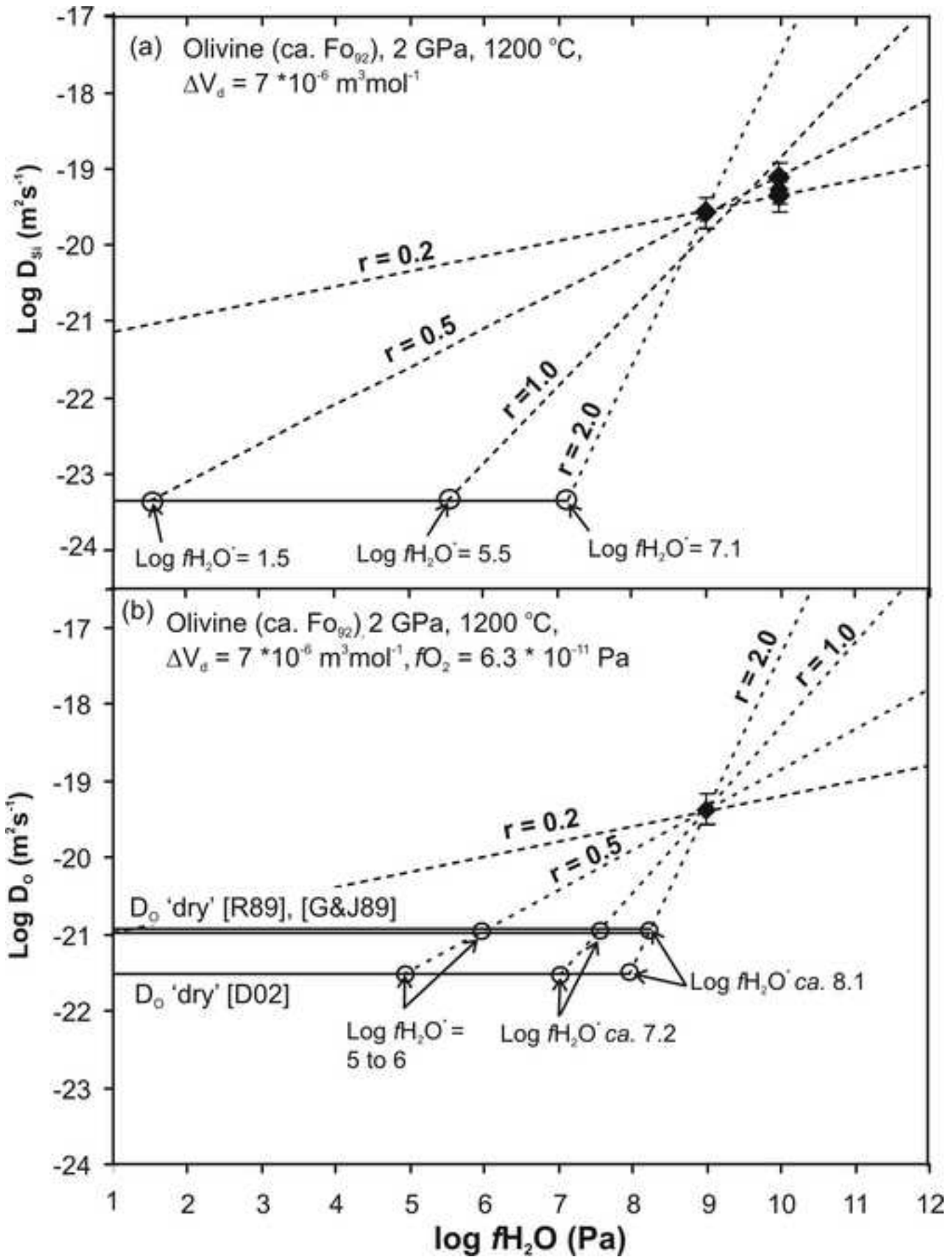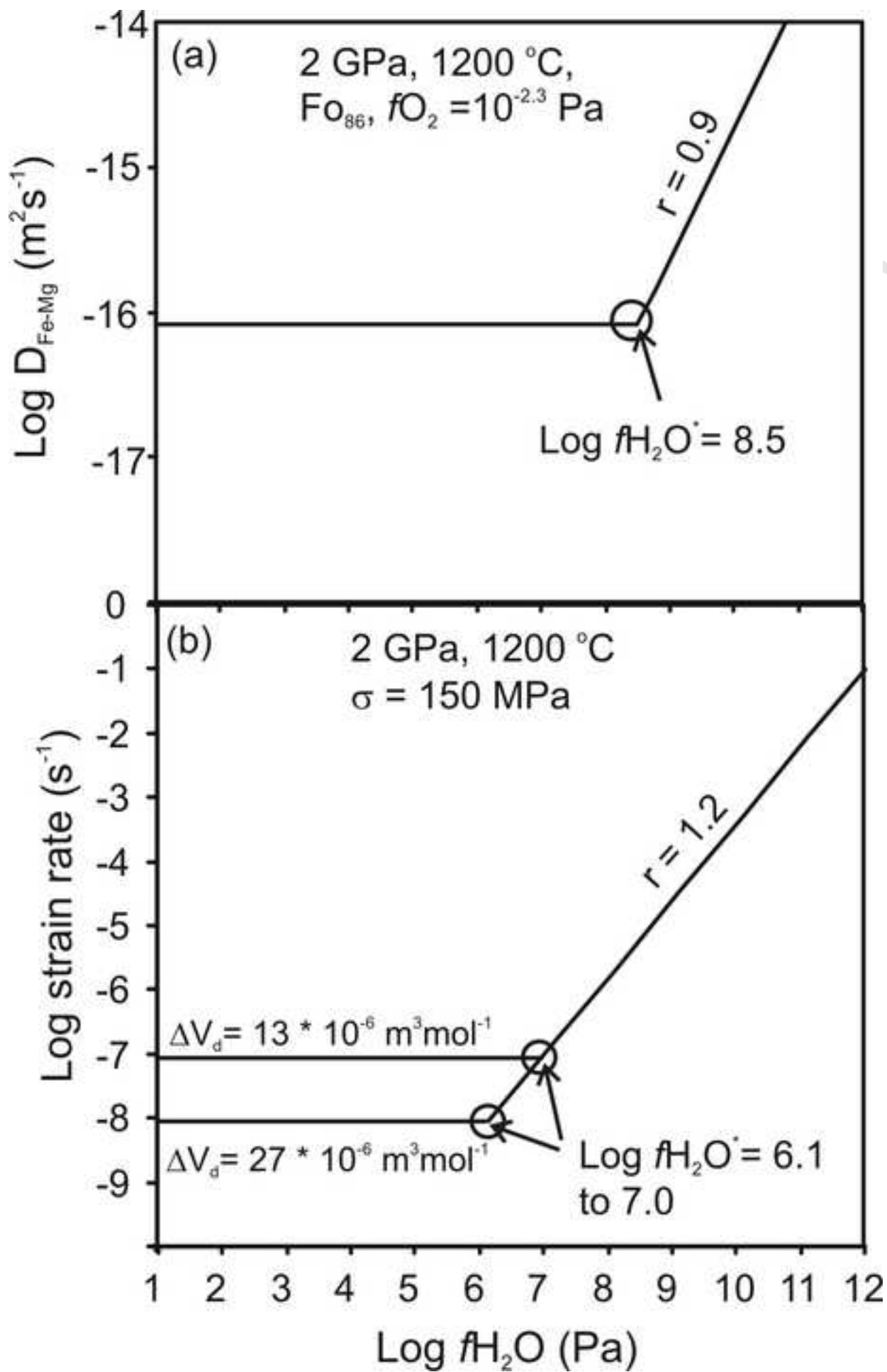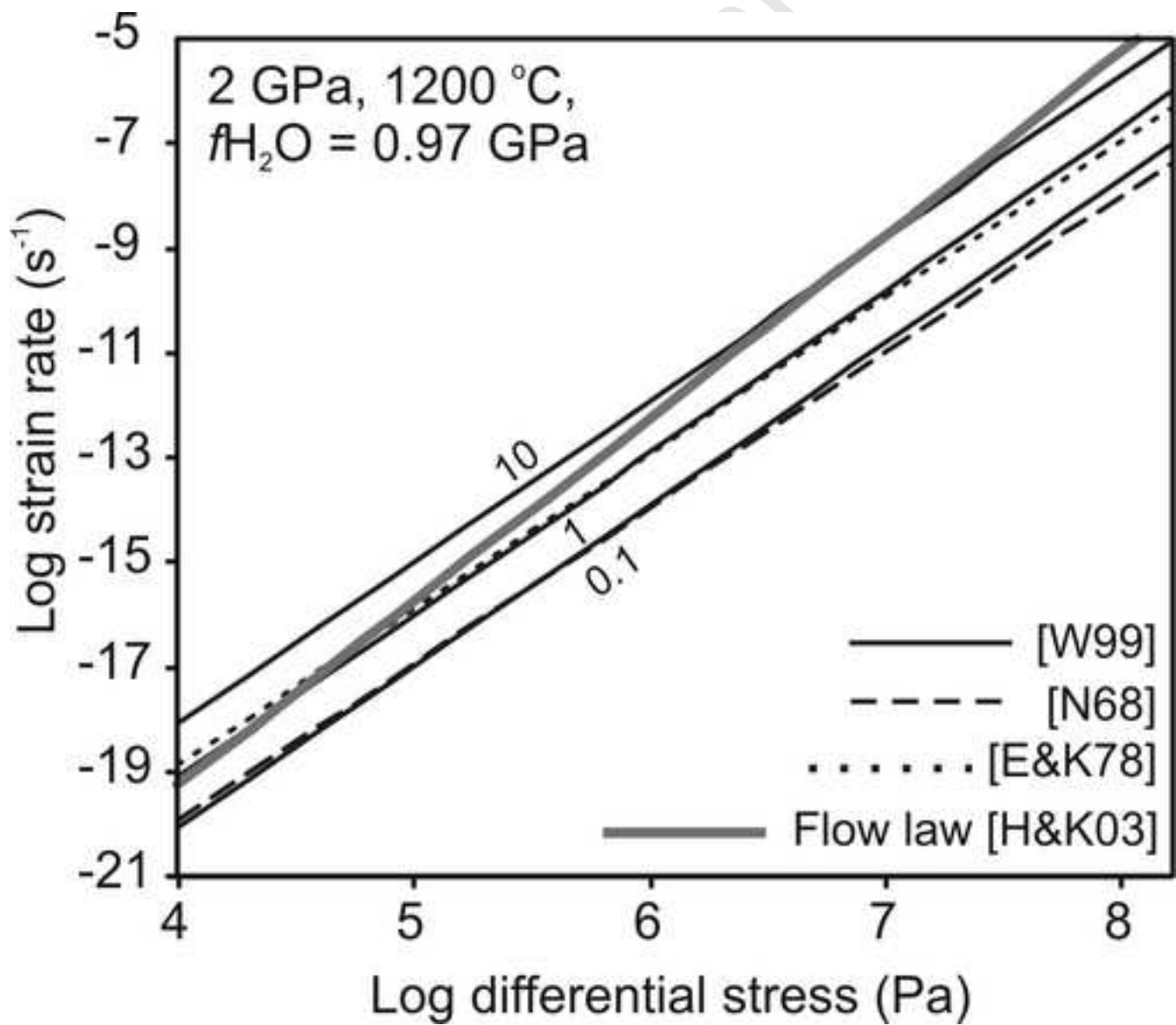
Table 1. Experimental conditions and diffusion coefficients determined in San Carlos Olivine (ca.Fo$_{92}$). All experiments at 2 GPa.

	orientation	T (^{o}C)	time in hours	H$_2$O ppm in olivine, measured	H$_2$O ppm in olivine, calculated #	fH$_2$O* GPa	Log fO$_2$* Pa	D$_{Si}$ (m^{2}s^{-1})	D$_O$ (m^{2}s^{-1})	Observations
ScOl25a	random	1350	6		51	0.89	-5.8	9.91•10^{-19}	8.96•10^{-19}	slow quench
ScOl25b	random	1350	6		51	0.89	-5.8	6.99•10^{-19}	1.79•10^{-18}	slow quench
scOl26a	23° with [001]	1300	14		45	0.91	-6.2	3.69•10^{-19}	6.73•10^{-19}	slow quench
scOl26b	23° with [001]	1300	14		45	0.91	-6.2	3.35•10^{-19}	5.92•10^{-19}	slow quench
ol4051b	$\perp$ [001]	1350	12		51	0.89	-5.8	2.90 •10^{-19}	1.07•10^{-18}	slow quench
ol4051a	$\perp$ [001]	1350	12		51	0.89	-5.8	2.30•10^{-19}	1.07•10^{-18}	slow quench
ol4052a	$\perp$ [001]	1250	20		40	0.94	-6.7	6.60•10^{-20}	2.07•10^{-19}	slow quench
ol4041	// [001]	1350	12	29	51	0.89	-5.8	2.30 •10^{-19}	1.01•10^{-18}	slow quench
ol4042	// [001]	1250	20	19	40	0.94	-6.7	7.50•10^{-20}	9.20•10^{-20}	slow quench
olF1-1	// [001]	1275	20	16	43	0.93	-6.5	1.18 •10^{-19}	1.77•10^{-19}	slow quench
olF1-1b	// [001]	1275	20	16	43	0.93	-6.5	1.57•10^{-19}	2.48•10^{-19}	slow quench
OLF1-3	// [001]	1200	48		35	0.97	-7.2	2.68•10^{-20}	4.19•10^{-20}	slow quench
ol40f14_2a1	// [001]	1200	48		> 370	> 9.4	ca. -3.9	5.37•10^{-20}		slow quench, brucite present
ol40f14_2a2	// [001]	1200	48		> 370	> 9.4	ca. -3.9	7.52•10^{-20}		slow quench, brucite present
ol40f14_2b1	// [001]	1200	48		> 370	> 9.4	ca. -3.9	4.29•10^{-20}		slow quench, brucite present
ol40f12_3a1	// [001]	1300	20	11	45	0.91	-6.2	4.10•10^{-19}	5.39•10^{-19}	slow quench
ol40f13_1a1	// [001]	1225	64	19	37	0.95	-7.0	5.96•10^{-20}		slow quench
ol40f13_1b1	// [001]	1225	64	19	37	0.95	-7.0	5.96•10^{-20}		slow quench
ol40f13_2a1	// [001]	1325	16	13	48	0.90	-6.0	6.63•10^{-19}		slow quench
ol40f13_2a2	// [001]	1325	16	13	48	0.90	-6.0	7.89•10^{-19}		slow quench
ol40f11_3a1si	// [001]	1300	14		45	0.91	-6.2	1.17•10^{-19}		slow quench
ol40f11-2a1	// [001]	1325	5		48	0.90	-6.0	1.58•10^{-19}		slow quench
Experiments to quantify the water contents present at run conditions										
14F_1	// [001]	1275	20	43		0.93 §	-6.6			fast quench
40F2TR	// [001]	1250	20	40		0.94 §	-6.7			fast quench
14F_5B	// [001]	1225	40	370		9.4 §	ca. -3.9			fast quench, brucite present

// means parallel to an axis, and $\perp$ means perpendicular to an axis. § water fugacity calculated using the measured OH concentration in olivine and the solubility equation of Zhao et al. (2004). * water and oxygen fugacities calculated using the fluid composition of quickly quenched samples as obtained from modeling their C-O-H fluid equilibria. # water content in the olivine calculated from water solubility equation of Zhao et al. (2004) and the fugacity obtained from fluid equilibria modeling results. For the samples with the highest fH$_2$O, the fO$_2$ was calculated from an fH$_2$O of 9.2 GPa because this is the maximum possible value that can be obtained using the presence of graphite and the equations of state for fluids mentioned in the text. It is worth noting that the fugacity of pure water from the EOS of Pitzer and Sterner (1994) used in the Zhao et al. (2004) calibration are about 5 % higher (at the investigated P and T) than that of Holloway (1981).

Table 2. Summary of experimentally determined kinetic parameters for various elements and phenomena (diffusion and deformation) in olivine

	Material	Crystal orientation	D_o (m^{2}s^{-1})	E (kJmol^{-1})	P (Pa)	fH$_2$O (GPa)$	fO$_2$ (Pa) $	fO$_2$ exponent	fH$_2$O exponent	ΔV · 10^{-6} (m^{3}mol^{-1})	D (m^{2}s^{-1}) or εdot (s^{-1}) at 1200 °C	Đwet/Đdry at 1200 °C, fO$_2$ corrected*	Đwet/Đdry at 1200 °C, fO$_2$ and P (2 GPa) corrected*	References and observations
Volume diffusion kinetic parameters and experimental conditions														
Silicon														
Water bearing														
Si	SC	// and ⊥ [001]	1.68 (±3.52) • 10^{-7}	358 ± 28	2 •10^9	0.97	6.3 • 10^{-8}		0.5 to 1		2.7 • 10^{-20}@	2.4 • 10^3	6.0 • 10^3	This study
Si	SC	// [001]			2 •10^9	9.4	1.2 • 10^{-4}				4.3 to 7.5 • 10^{-20}	6.8 • 10^3	17 • 10^3	This study
Dry'														
Si	SC	// and ⊥ [001]	1.9 • 10^{-13}	291 ± 15	10^5		10^{-5} to 10^{-1}	-1/5		0.7 (±2.3)				Houlier et al. (1990), ΔV from Béjina et al. (1999)
Si	Fo$_{93}$	// [001]	6.3 • 10^{-5}	529 ± 41	10^5		10^{-4}				1.1 • 10^{-23}			Dohmen et al. (2002)
Si pp	Fo$_{93}$	// [001]		540	2 •10^9					7.0 €	4.5 • 10^{-24}			Dohmen et al. (2002) normalized for P
Oxygen														
Water bearing														
O	SC	// and ⊥ [001]	1.43 (±1.80) • 10^{-4}	437 ± 17	2 •10^9	0.97	6.3•10^{-8}		ca. 0.5		4.6 • 10^{-20}			This study
Onn	SC	// and ⊥ [001]	1.2 • 10^{-6}	324	2 •10^9	0.97	10^{-4}	1/4%			3.3 • 10^{-19}			This study, constant fO$_2$
Dry'														
O	SC	// [100]	2.6 • 10^{-10}	266 ± 11	10^5		10^{-4}	1/5			1.5 • 10^{-20}	22		Ryerson et al. (1989)
Opp	SC	// [100]		277	2 •10^9		10^{-4}			7.0 €	6.2 • 10^{-21}		54	Ryerson et al. (1989) normalized for P
O	SC	// [001]	6.7 • 10^{-6}	318 ± 17	10^5		10^{-4}	1/3			3.1 • 10^{-20}	11		Gérard and Jaoul (1989)
Opp	SC	// [001]		329	2 •10^9		10^{-4}			7.0 €	1.3 • 10^{-20}		27	Gérard and Jaoul (1989) corrected for P
O	Fo$_{93}$	// [001]	4.6 • 10^{-9}	338 ± 14	10^5		10^{-4}				4.7 • 10^{-21}	70		Dohmen et al. (2002b)
Opp	Fo$_{93}$	// [001]		349	2 •10^9		10^{-4}			7.0 €	1.9 • 10^{-21}		173	Dohmen et al. (2002b) corrected for P
Iron-magnesium														
Water saturated														
Fe-Mg	Fo$_{86}$	// [001]	10$^{-14.8(±2.7)}$	220 ± 60	10^5	0.97	10$^{-2.3}$ £		0.9 ±0.3	16 (±6.0)	2.2 • 10^{-16} (at 2 GPa)			Hier-Majumder et al. (2005)
Dry'														
Fe-Mg	Fo$_{86}$	// [001]	10$^{-9.2}$#	200 #	10^5		10$^{-2.3}$	1/6 #		7.0	1.2 • 10^{-16} (at 2 GPa)		2	Dohmen and Chakraborty (2007), ΔV from Holzapfel et al. (2007)
Dislocation creep kinetic parameters and experimental conditions														
Water-bearing, constant OH	SC grain aggregates			480 ± 40	10^5	0.97			1.2	11	2.3 • 10^{-5} (at 2 GPa)		304 to 1321	Hirth and Kohlstedt (2003), σ=150 MPa
Dry	SC grain aggregates			530 ± 40	10^5					13 to 27	1.7 to 7.4 • 10^{-8} (at 2 GPa)			Hirth and Kohlstedt (2003), σ=150 MPa

Notes and keys to the symbols: ⊥ means perpendicular to an axis and // parallel to an axis. The dry data for Si here refers to Dohmen et al. (2002b). $ these values are for T = 1200 °C and 2 GPa (where applicable) and are those used in the calculation of the rate constants.*normalization not always necessary. εdot = strain rate. s= differential stress. Đ stands for diffusivity and strain rate. @ measured data not calculated with the kinetic parameters. SC = San Carlos olivine (Fo$_{92}$). € this activation volume is taken to be the same as that for Fe-Mg (Holzapfel et al., 2007). % value assumed intermediate between the 1/3 and 1/5 exponents determined by Gérard and Jaoul (1989) and Ryerson et al. (1989), respectively. # values vary depending on fO$_2$ (see Dohmen and Chakraborty, 2007). £ this fO$_2$ corresponds to the Ni-NiO buffer (calibration of Huebner and Sato, 1970) used by Hier-Majumder et al. (2005) at the appropriated P, T.

Table 3. Log water fugacity values ($f\text{H}_2\text{O}^*$) for the wet to dry transition in olivine for various transport phenomena and 3 representative water fugacity exponents at 1200 ^{o}C and 2 GPa.

	$f\text{H}_2\text{O}$ exponent r			
Log $f\text{H}_2\text{O}^*$ (Pa) and H_2O ppm in olivine	2	1	1/2	1/5
Si volume diffusion	7.1 to 8.1 0.5 to 5	5.2 to 6.2 <0.1	1.5 to 2.5 <0.1	<-10 <<0.1
O volume diffusion	7.9 to 8.4 3 to 9	6.9 to 7.8 0.3 to 2	5.1 to 6.4 < 0.1	<1 < 0.1
Fe-Mg volume diffusion		8.5* 11		
Dislocation creep		6.1 to 7.0** <0.1 to 0.4		

Notes and keys to the symbols: For Si and O diffusion the variation on Log $f\text{H}_2\text{O}^*$ values correspond to varying ΔV_d from 0 to of $7 \cdot 10^{-6}$ $\text{m}^3\text{mol}^{-1}$. For oxygen diffusion the values were calculated at the experimental conditions ($f\text{O}_2 = 6.3 \cdot 10^{-8}$ Pa) and the variation also includes the difference between the dry diffusion data of Gérard and Jaoul (1989), Ryerson et al. (1989), and Dohmen et al. (2002b). * Exponent is 0.9 (Hier-Majumder et al., 2005). The transition of dry to wet for Fe-Mg was obtained at Fo$_{86}$, NNO ($f\text{O}_2 = 10^{-2.3}$ Pa) and using the equation for dry diffusion of Dohmen and Chakraborty (2007). **Exponent is 1.2, and the variation arises from using ΔV_d of 13 to 27 $\cdot 10^{-6}$ $\text{m}^3\text{mol}^{-1}$, using values for a constant water content using the power law parameters in Hirth and Kohlstedt (2003) with $\sigma = 150$ MPa.

Table 4. Dependencies of point defect concentrations on water fugacity for three charge neutrality conditions. The numbers are the water fugacity exponent r.

	$[(OH)^\bullet_O]$	$[\{(OH)^\bullet_O\text{-}V''_{Me}\}']$	$[\{2(OH)^\bullet_O\text{-}V''_{Me}\}^x]$	$[V^{\bullet\bullet}_O]$	$[O''_i]$	$[V_{Si}''''']$	$[Si_i^{\bullet\bullet\bullet\bullet}]$	$[H_{Si}''']$	$[(2H)_{Si}'']$	$[(3H)_{Si}']$	$[(4H)_{Si}^x]$
$[(OH)^\bullet_O] = 2[V''_{Me}]$	1/3	2/3	1	-1/3	1/3	2/3	-2/3	1	4/3	5/3	2
$[(OH)^\bullet_O] = [\{(OH)^\bullet_O\text{-}V''_{Me}\}']$	1/2	1/2	1	0	0	0	0	1/2	1	3/2	2
$[Fe^\bullet_{Me}] = [\{(OH)^\bullet_O\text{-}V''_{Me}\}']$	3/4	1/4	1	1/2	-1/2	-1	1	-1/4	1/2	5/4	2

Note: $[H_{Si}''']$ stands for $[\{(OH)\bullet_O\text{-}V''''_{Si}\}''']$ and analogous abbreviations have been used for the other Si vacancy complexes. Exponents taken from Kohlstedt and Mackwell (1998 and 1999), Kohlstedt (2006), and Karato (2006). Shaded ones are those that agree most with the diffusion data.

Table 5. Diffusion coefficients (m^2s^{-1}) and calculated point defect concentrations at 1200 ^{o}C, 2 GPa, fO_2 = $10^{-2.3}$ Pa.		
	Dry	fH_2O = 0.97 GPa
D_{Fe-Mg}	$1.2 \cdot 10^{-16}$	$2.2 \cdot 10^{-16}$
D_{Si}	$4.5 \cdot 10^{-24}$	$2.7 \cdot 10^{-20}$
$[V_{Me}]$	$8.8 \cdot 10^{-5}$	$4.4 \cdot 10^{-4}$
$[V_{Si}]$	$3.5 \cdot 10^{-12}$	$5.3 \cdot 10^{-8}$